

# Deep thermalization under charge-conserving quantum dynamics

Rui-An Chang,<sup>1</sup> Harshank Shrotriya,<sup>2</sup> Wen Wei Ho,<sup>2,3</sup> and Matteo Ippoliti<sup>1</sup>

<sup>1</sup>*Department of Physics, The University of Texas at Austin, Austin, TX 78712, USA*

<sup>2</sup>*Centre for Quantum Technologies, National University of Singapore, Singapore 117543*

<sup>3</sup>*Department of Physics, National University of Singapore, Singapore 117551*

“Deep thermalization” describes the emergence of universal wavefunction distributions in quantum many-body dynamics, appearing on a local subsystem upon measurement of its environment. In this work, we study in detail the effect of continuous internal symmetries and associated conservation laws on deep thermalization. Concretely, we consider quantum spin systems with a  $U(1)$  symmetry associated with the conservation of magnetization (or ‘charge’), and analyze how the choice of initial states (specifically, their degree of charge fluctuations) and the choice of measurement basis (specifically, whether or not it can reveal information about the local charge density) determine the ensuing universal wavefunction distributions. We find a rich set of possibilities. First we focus on the case of a random state of well-defined charge subjected to charge-revealing measurements, and rigorously prove that the projected ensemble approaches a direct sum of Haar ensembles in the charge sectors of the subsystem of interest. We then analytically derive the limiting wavefunction distributions for more general initial states and measurement bases, finding results that include the Haar ensemble, the “Scrooge ensemble” (a distortion of the Haar ensemble by a density matrix), and the “generalized Scrooge ensemble” (a stochastic mixture of multiple Scrooge ensembles). These represent nontrivial higher-moment generalizations of the Gibbs state, and notably can depend on the entire charge distribution of the initial state, not just its average. Our findings demonstrate a rich interplay between symmetries and the information extracted by measurements, which allows deep thermalization to exhibit a range of universal behaviors far beyond regular thermalization.

## CONTENTS

I. Introduction	1	2. General structure of the moment operators	22
II. Review of projected ensemble and overview of deep thermalization with symmetries	3	3. Charge-revealing measurements on general states	23
A. Projected ensemble	3	4. Charge-non-revealing measurements on symmetric states	26
B. Deep thermalization	3	C. Constraints from locality of the dynamics	29
III. Projected ensemble of a random $U(1)$ -symmetric state	6	D. Choice of parameters for numerical simulations	30
IV. Theory of universal limiting ensembles for general initial states and measurement bases	7	E. Numerical results for higher moments	30
A. Maximally charge-revealing measurements	8		
B. Charge-non-revealing measurements	10		
C. Partially charge-revealing measurements	10		
V. Numerical results	10		
A. Maximally charge-revealing measurements	11		
B. Charge non-revealing measurements	13		
C. Higher moments	14		
VI. Discussion	14		
Acknowledgments	15		
References	15		
A. Proof of Theorem 1	18		
B. Limiting form of the projected ensemble at late time	21		
1. Setup	21		

## I. INTRODUCTION

The advent of quantum computers and simulators has opened up new ways to address fundamental questions in quantum many-body physics. Among these questions is the emergence of irreversible equilibration from the reversible unitary dynamics of isolated quantum many-body systems. This apparent paradox is resolved by recognizing that equilibration within an isolated quantum system should be considered only within a *local* subsystem, such that there is a large complementary subsystem (the ‘bath’) with which the former can exchange information, energy, and any other conserved quantities. Mathematically, this is captured by the reduced density matrix  $\rho_A = \text{Tr}_B(|\Psi\rangle\langle\Psi|)$  — a description of the local subsystem  $A$  in which the complement  $B$  (‘the bath’) is ignored. This state quickly becomes mixed due to the build-up of quantum entanglement, and typically converges to the form of a Gibbs state, which is universal and insensitive to details of the initial state, up to information about

any conserved quantities. This is what is conventionally known as ‘quantum thermalization’ [1–6].

However, in modern quantum simulator experiments, it is possible for an observer to obtain information about *all* of the system’s degrees of freedom at once, e.g. by single-atom resolved fluorescence. This yields ‘snapshots’ of the different classical configurations that the entire system can be found in, typically in the form of bit-strings (each bit denoting, e.g., the occupation of a lattice site). In this scenario, the separation between a subsystem of interest  $A$  and the bath  $B$  is arbitrary and artificial, and even if we wish to study local properties of  $A$ , we need not discard the data from  $B$ . Indeed, one can study the local equilibration of a quantum many-body system *conditioned* upon the measurement outcome of the complement, as was done in Refs. [7–15]. The relevant theoretical construct is the *projected ensemble* — an ensemble of pure states of  $A$ , conditioned and weighted by the outcomes of projective measurements performed on the bath  $B$ , as sketched in Fig. 1. One may view the projected ensemble as a particular, physically motivated unraveling of the reduced density matrix into a set of constituent pure states.

The novelty and interest in the projected ensemble lies in the fact that it can exhibit new forms of universal equilibration physics, going beyond the framework of standard quantum thermalization, and thus collectively dubbed “deep thermalization”. Initial studies concentrated on the conceptually simplest case of dynamics without conservation laws or at infinite temperature [8]. There it was found (numerically, analytically, and also experimentally [7]) that the projected ensemble tends at late times to a distribution in which quantum states are drawn uniformly randomly from the Hilbert space, i.e., the Haar distribution [16]. In quantum information jargon, the projected ensemble at late but finite times is said to form a ‘quantum state-design’ [17, 18]. This was later proven in various dynamical settings including ‘maximally-chaotic’ systems in one spatial dimension [9, 10, 19] and random-matrix models [11, 20]. In comparison, studies of quantum dynamics with symmetries and associated conservation laws — such as energy conservation generated by a time-independent Hamiltonian — are at a more preliminary stage. It has been claimed that the projected ensemble does still converge to a universal limiting form, namely one in which the Haar distribution is ‘distorted’ by the conserved charges [8, 14]. In either case, the emergence of these universal distributions has been argued to be underpinned by *maximum-entropy principles* similar to, but going beyond, the second law of thermodynamics [14], which endow them with special quantum information theoretic properties. We note also that recent works have generalized the findings of deep thermalization beyond the arena of quantum spin chains (which is the setting of the aforementioned works), to the physically distinct arenas of fermionic systems [13] and bosonic continuous-variable quantum systems [15]. While the form of the limiting distributions changes, it

was found that they still nevertheless follow the same maximum entropy principles.

In this work, we substantially expand on this nascent understanding of the role of conservation laws in deep thermalization. Concretely, we focus on quantum many-body spin systems with an on-site  $U(1)$  symmetry associated to the conservation of a component of total magnetization (which we also refer to as ‘charge’ or ‘particle number’). The presence of such a symmetry and associated conservation law has been shown to significantly affect thermalization, operator spreading, and the dynamics of entanglement in quantum many-body systems [21–29]. The effect of symmetry on deep thermalization turns out to be just as striking: we find a rich variety of limiting ensembles depending on the charge fluctuations in the initial state, as well as on the choice of measurement basis, particularly how much information it reveals about the value of the conserved charge. Importantly, while they depend on some information about the initial state, these limiting ensembles are still universal, in the sense that they depend on only a small (linear in system size) number of parameters, such as the distribution of charges of the initial state. These ensembles may be thought of as higher-moment generalizations of the Gibbs state  $\rho \propto e^{\beta\mu\hat{N}}$  in standard thermalization; while the fugacity  $e^{\beta\mu}$  in the Gibbs state remembers the average charge in the initial state, the universal ensembles in deep thermalization may remember the whole charge distribution.

Our results are backed by analytical arguments and calculations, as well as extensive numerics performed on a well-explored testbed for symmetry in chaotic many-body dynamics:  $U(1)$ -symmetric random quantum circuits [21–23, 30]. We note that while higher-moment statistics and formation of quantum state designs in systems with  $U(1)$  symmetry have recently been considered in Refs. [31–35], our work is the first to study these concepts in the context of the projected ensemble and of deep thermalization, where randomness emerges from quantum measurements rather than from the choice of random unitary interactions.

The rest of our article is structured as follows. In Sec. II, we briefly review the concepts of the projected ensemble and deep thermalization, focusing in particular on prior results on energy-conserving systems. In Sec. III we present our first main result: a rigorous proof of deep thermalization for Haar-random states within a fixed charge sector. Building on this result, we present a general theory for the limiting form of the projected ensemble under more general initial states and measurement bases in Sec. IV, and present supporting numerical evidence in Sec. V. We conclude by discussing our results and possible avenues for future work in Sec. VI.

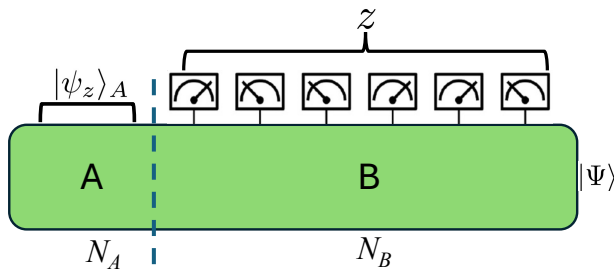


Figure 1. Construction of the projected ensemble in a one-dimensional spin chain consisting of subsystem  $A$  and bath  $B$ .  $|\Psi\rangle$  is a many-body wavefunction on the entire system  $AB$ .  $|\psi_z\rangle_A$  is the projected state of the subsystem  $A$  appearing in the projected ensemble. It is the conditional state on  $A$  after a measurement with outcome  $z$  is performed on the bath  $B$ , and occurs with Born probability  $p(z)$ .

## II. REVIEW OF PROJECTED ENSEMBLE AND OVERVIEW OF DEEP THERMALIZATION WITH SYMMETRIES

For completeness, we begin by reviewing the theoretical foundations of the projected ensemble framework first introduced in Refs. [7, 8], as well as the phenomenon of deep thermalization that can arise within the framework. Readers who are familiar with these topics may proceed directly to our results, Sec. IV.

### A. Projected ensemble

Consider a pure quantum many-body state  $|\Psi\rangle$  on  $N$  qubits which is partitioned into two subsystems  $A$  and  $B$  with  $N_A$  and  $N_B$  qubits respectively, as shown in Fig. 1. We assume  $N_A \ll N_B$ , and are interested in the state of the region  $A$ , which we take to be geometrically local. The complementary region  $B$  thus plays the role of a “bath”—though crucially we assume that some information about its particular state can be obtained through a quantum measurement, for example through a projective measurement in the computational basis (though we will relax this assumption in our work). This allows us to generate an ensemble  $\mathcal{E}$  of pure states  $|\psi_z\rangle_A$  on the subsystem  $A$ , each of which is correlated with a measurement outcome  $z \in \{0, 1\}^{N_B}$  on the bath that occurs with probability  $p(z)$ , and physically represents the *conditional* post-measurement state on  $A$ . This ensemble,

$$\mathcal{E} \equiv \{(p(z), |\psi_z\rangle_A) : z = 1, \dots, d_B = 2^{N_B}\}, \quad (1)$$

is called the projected ensemble [7, 8]. Precisely, we have

$$p(z) = \|\langle z | \Psi \rangle_{AB}\|^2, \quad |\psi_z\rangle_A = \frac{B \langle z | \Psi \rangle_{AB}}{\sqrt{p(z)}}. \quad (2)$$

One may view a state ensemble as a probability distribution over the Hilbert space of  $A$ , and as such can be

characterized by its statistical moments. The  $k^{\text{th}}$  ‘moment operator’ of the projected ensemble  $\mathcal{E}$ , capturing all  $k$ -point correlations within the ensemble, is given by

$$\rho_{\mathcal{E}}^{(k)} = \sum_z p(z) (|\psi_z\rangle \langle \psi_z|)^{\otimes k}, \quad (3)$$

where the subscript  $A$  is omitted for brevity.  $\rho^{(k)}$  can be understood as a density matrix in a  $k$ -fold replicated Hilbert space  $\mathcal{H}_A^{\otimes k}$ , describing  $k$  copies of a state randomly drawn from the ensemble. It can be readily checked that the mean,  $k = 1$ , is just the reduced density matrix of subsystem  $A$ :

$$\rho_{\mathcal{E}}^{(1)} = \rho_A = \text{Tr}_B(|\Psi\rangle \langle \Psi|). \quad (4)$$

A quantity that can be represented by the projected ensemble but not by the reduced density matrix is, for example, the variance of  $\langle O \rangle_z = \langle \psi_z | O | \psi_z \rangle$ , the *conditional* expectation value of an operator  $O$  on  $A$  given the outcome  $z$  of measurements performed on  $B$ :

$$\begin{aligned} \text{var}_{z \sim \mathcal{E}}[\langle O \rangle_z] &= \mathbb{E}_{\mathcal{E}}[\langle O \rangle_z^2] - \mathbb{E}_{\mathcal{E}}[\langle O \rangle_z]^2 \\ &= \sum_z p(z) \langle \psi_z | O | \psi_z \rangle^2 - \text{Tr}(O \rho)^2 \\ &= \text{Tr}[(\rho_{\mathcal{E}}^{(2)} - \rho^{\otimes 2}) O^{\otimes 2}]. \end{aligned} \quad (5)$$

This quantity can thus be expressed as the expectation value of a “higher-order” observable in a two-fold replicated Hilbert space. Similarly, higher moment fluctuations of  $\langle O \rangle_z$  would involve an expectation value on the state  $\rho_{\mathcal{E}}^{(k)}$  on the  $k$ -fold replicated Hilbert space. This example also highlights the difference between  $\rho^{(k)}$  ( $k$ -th moment operator) and  $\rho^{\otimes k}$  ( $k$  copies of the first-moment operator, i.e. the reduced density matrix).

Measuring higher-order observables like the one in Eq. (5) is nontrivial, but can be done with either a large amount of experimental sampling or the assistance of classical computation [36–38]. The quantity in Eq. (5) has in fact been measured in a Rydberg-atom based quantum simulator [7].

### B. Deep thermalization

The standard theoretical approach to thermal equilibrium in isolated many-body systems is based on expectation values of local observables at late times. This is captured by the reduced density matrix  $\rho_A$  for a local subsystem, obtained by tracing out the degrees of freedom in  $B$  which now plays the role of a thermal bath:

$$\langle O_A(t) \rangle = \text{Tr}(O_A \rho_A(t)), \quad \rho_A(t) = \text{Tr}_B(|\Psi(t)\rangle \langle \Psi(t)|). \quad (6)$$

This notion of thermalization (which we will call ‘standard quantum thermalization’) is thus equivalent to the approach of the reduced density matrix to an equilibrium ensemble,  $\rho_A(t) \rightarrow \text{Tr}_B(\rho_{\text{eq}})$ . The thermal density matrix  $\rho_{\text{eq}}$  has the form of a Gibbs state with a

Lagrange multiplier corresponding to each globally conserved quantity—e.g., energy, charge, etc. If energy is the only conserved quantity, we have

$$\rho_{\text{eq}} \propto e^{-\beta H} \quad (7)$$

where  $\beta$  is the inverse temperature.

Since, as we saw,  $\rho_A$  equals the first moment of the projected ensemble  $\rho^{(1)}$ , the statement of standard quantum thermalization is about the universal limiting form of the *first moment* of the projected ensemble. It is natural to ask whether this approach toward a universal equilibrium form extends to higher moments as well, and to the entire distribution more generally. The idea of *deep thermalization* is precisely that the full projected ensemble  $\mathcal{E}$  does converge, at late time in dynamics, to a universal form that we will denote as the ‘target’ ensemble  $\mathcal{E}_{\text{target}}$ . As we will see below, the target ensemble can depend on some coarse features of the dynamics and of the initial state, but should otherwise be insensitive to microscopic details and thus universal. Quantitatively, convergence to a given target ensemble  $\mathcal{E}_{\text{target}}$  over the course of quantum dynamics can be captured at the level of each statistical moment  $k$  by the distance measure

$$\Delta^{(k)} = \frac{1}{2} \|\rho_{\mathcal{E}}^{(k)} - \rho_{\text{target}}^{(k)}\|_{\text{tr}}. \quad (8)$$

Here  $\|\cdot\|_{\text{tr}}$  is the trace norm, which has an operational meaning in terms of optimal quantum state discrimination. The vanishing of  $\Delta^{(k)}$  as a function of time in dynamics, for a suitable choice of target ensemble and moment  $k \geq 2$ , is what defines deep thermalization. Standard quantum thermalization is recovered for  $k = 1$  and using the appropriate Gibbs state as the target.

### 1. Absence of conservation laws

In the absence of symmetries or other constraints, it is reasonable to conjecture that the universal ensemble achieved in deep thermalization should feature all states in the Hilbert space on an equal footing. This property can be better formalized mathematically as *unitary invariance* of the limiting distribution, and leads to the definition of the Haar ensemble [16]. At the level of the first moment, this immediately implies equilibration of local subsystems to the maximally-mixed state,  $\rho_A \xrightarrow{t \rightarrow \infty} \mathbb{I}_A/2^{N_A}$ , corresponding to Eq. (7) with infinite temperature ( $\beta = 0$ ), in line with expectations from standard quantum thermalization. However, this also nontrivially predicts the form of all higher moments,  $\rho_{\mathcal{E}}^{(k)}(t) \xrightarrow{t \rightarrow \infty} \rho_{\text{Haar}}^{(k)}$ , where  $\rho_{\text{Haar}}^{(k)}$  are the moments of the Haar ensemble, whose forms are known analytically. In this specific case, there is a dedicated nomenclature for the condition  $\Delta^{(k)} \leq \epsilon$ : the ensemble is said to form an “ $\epsilon$ -approximate quantum state  $k$ -design” [16–18, 39]. This concept is of interest in quantum information science, specifically in the context of randomized algorithms

or protocols, where it serves as an efficient alternative to the Haar distribution [40–43].

### 2. Presence of conservation laws

In the presence of symmetries and associated conservation laws, the picture becomes substantially richer and more complex. This complication arises from two fronts: (i) the distribution of the conserved quantity in the initial state, and (ii) the nature of the measurements on the ‘bath’  $B$ , namely whether or not they reveal information about the conserved quantity.

The first aspect is, to an extent, already present in the picture of conventional thermalization: the system retains memory of the value of any conserved quantities in the initial state, which at late time is stored in the various Lagrange multipliers (inverse temperature, chemical potential, etc) of the Gibbs state, Eq. (7). Since the Gibbs state sets the first moment of the projected ensemble, this immediately raises the question of what the appropriate target ensemble should be away from infinite temperature—where  $\rho^{(1)} \neq \mathbb{I}_A/d_A$  and thus the Haar ensemble is not a suitable candidate. An important point to note in this regard is that the equilibrium density matrix  $\rho_{\text{eq}}$  depends only on the *expectation value* of the conserved quantities in the initial state, not on their *quantum fluctuations*. The latter are scrambled non-locally across the whole system ( $AB$ ) and thus rendered inaccessible to observations on the local subsystem  $A$ . However, this is not necessarily true in deep thermalization. Indeed, the projected ensemble contains information that goes beyond local expectation values—it captures higher statistical moments and contains global data via the measurement outcomes on  $B$ . It appears plausible, then, that the universal limiting ensembles of deep thermalization might depend on the whole distribution of conserved quantities in the initial state, and not just their expectation values. This already opens up a much wider variety of possibilities for universality compared to the scenario of standard thermalization.

The second aspect, i.e., the dependence on the choice of measurement basis of  $B$ , does not have an analog in conventional thermalization, where the bath is simply discarded (traced out). In the absence of conservation laws, as we discussed earlier, the limiting ensemble is found to be the Haar ensemble regardless of the choice of local measurement basis. However, in the presence of a conserved quantity  $Q$  with a local density  $q_i$  (i.e.,  $Q = \sum_i q_i$  with each  $q_i$  operator supported on a finite neighborhood of qubit  $i$ ), the choice of measurement basis has distinct physical consequences.

Let us focus for concreteness on local product-state measurement bases, where each qubit is measured along some direction  $\hat{n}$  in the Bloch sphere. Measuring the operator  $\hat{n} \cdot \vec{\sigma}_i$  might reveal information about the value of charge densities  $q_j$  at neighboring locations  $j$ . Specifically, we may decompose each measured operator  $\hat{n} \cdot \vec{\sigma}_i$



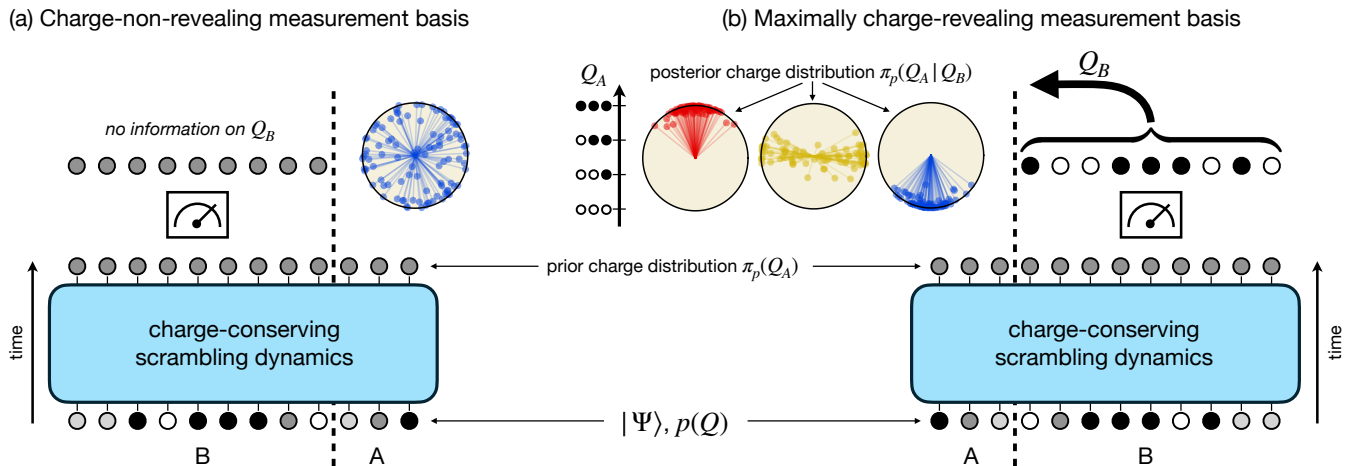


Figure 2. Diagram summarizing the effect of different measurement bases on deep thermalization under charge-conserving dynamics. (Bottom panels) An input state  $|\Psi\rangle$  with a given distribution of charge  $p(Q)$  (the probability distribution of charge) evolves under chaotic charge-conserving dynamics. Small circles represent qubits; the color represents the expectation value of the local charge density—white and black are 0 and 1, shades of gray are superpositions. At late times the charge on subsystem  $A$  reaches a stationary distribution,  $\pi_p(Q_A)$ . (a) The bath  $B$  is measured in a charge-non-revealing basis. Such a measurement does not update our knowledge of  $Q_A$ . Thus, a projected ensemble consistent with the prior distribution  $\pi_p(Q_A)$  is formed, sketched in the top right (the many-body Hilbert space of  $A$  is schematically represented as a sphere for simplicity, with dots representing projected states). (b) The bath  $B$  is measured in a maximally charge-revealing basis. Here the measurement outcome on  $B$  informs us as to the value of  $Q_B$ , and we can thus update our knowledge of  $Q_A$  to a ‘posterior’ distribution  $\pi_p(Q_A | Q_B)$ . This effectively splits the projected ensemble into multiple ensembles, one for each value of  $Q_B$ , distributed differently across the charge sectors of the Hilbert space. Qualitative sketches for the three different values of  $Q_B$  are shown in the top left spheres (the vertical coordinate indicates different  $Q_A$  charge sectors).

into a basis of operators that contains the conserved densities  $\{q_j\}$ :  $\hat{n} \cdot \vec{\sigma}_i = \sum_j \alpha_{ij} q_j + (\text{orthogonal operators})$ ; then, depending on the overlap coefficients  $\{\alpha_{ij}\}$ , the measurement outcome  $\hat{n} \cdot \vec{\sigma}_i = \pm 1$  may correlate non-trivially with the total value of the conserved quantity on  $B$ ,  $Q_B = \sum_{j \in B} q_j$ . More generally, a complete measurement on  $B$  provides information on  $2^{N_B}$  distinct operators,  $|b\rangle\langle b|$ , where  $b \in \{0, 1\}^{N_B}$  indexes the measurement basis; each of these may in principle correlate with  $Q_B$ . This has an important effect on deep thermalization, since this knowledge about the conserved quantity in the bath,  $Q_B$ , can translate into knowledge of the charge on the local subsystem,  $Q_A$ . For instance, if the total charge  $Q$  is known and our measurement of  $B$  indicates an unusually small value of  $Q_B$ , then the post-measurement state of  $A$  must have an unusually large value of  $Q_A$  to compensate.

Different local measurement bases will generally provide different amounts of information about the conserved quantity. In special cases that will be relevant to this work, it is possible to span the entire range from ‘non-revealing’ to ‘maximally revealing’ bases. A ‘non-revealing’ basis is one where the local measurements are perfectly uncorrelated with the conserved quantity,  $\langle b | q_j | b \rangle = 0$  for all basis vectors  $b$  and local densities  $q_j$ . In this case the measurement outcome on  $B$  does not systematically bias the post-measurement state toward some different region of Hilbert space. This is sketched

in Fig. 2(a). On the opposite end, a ‘maximally revealing’ basis is one where  $q_i = \hat{n} \cdot \vec{\sigma}_i$ —i.e., we measure the conserved density directly (possible only when the symmetry is on-site). In this case we expect different measurement outcomes to have strong, systematic impacts on the post-measurement states and hence on the limiting forms of the projected ensemble, as sketched in Fig. 2(b).

These behaviors have been recently investigated primarily in the case of energy-conserving, Hamiltonian systems (though consistent results were found also for symmetries other than time translation, such as fermionic parity [12] or spatial symmetries [44]). With energy conservation, the first moment of the projected ensemble should converge to the appropriate Gibbs state  $\text{Tr}_B(e^{-\beta H})$ , with an average energy dictated by the inverse temperature  $\beta$ . The conserved quantity (energy) has a local density given by the individual Hamiltonian terms:  $H = \sum_i h_i$ . Ref. [8] focused on the special case of a Hamiltonian  $H$  that admits an ‘energy non-revealing basis’. This is the case when  $H$  (in what follows we take the case of a Hamiltonian on many qubits as an example) features only two types of Pauli matrices, for example  $X$  and  $Y$  like in the mixed-field Ising model  $H = J \sum_i X_i X_{i+1} + h \sum_i X_i + g \sum_i Y_i$ , so that  $\langle z | h_i | z \rangle = 0$  for all sites  $i$  and all computational basis states  $z \in \{0, 1\}^N$ . Under this condition, it was found that the projected ensemble is well described by the so-called *Scrooge ensemble* [45]. The Scrooge ensemble

ble, which is a particular unraveling of a density matrix  $\rho$  into pure states, can be characterized via a two-step procedure termed ‘ $\rho$ -distortion’ of the Haar ensemble [46, 47]:

$$\mathcal{E}_{\text{Scrooge}}[\rho] = \left\{ \frac{\rho^{1/2} |\psi\rangle}{\|\rho^{1/2} |\psi\rangle\|} : d\psi = d_A \langle \psi | \rho | \psi \rangle d\psi_{\text{Haar}} \right\}. \quad (9)$$

In words, first a random state is drawn from the measure<sup>1</sup>  $d_A \langle \psi | \rho | \psi \rangle d\psi_{\text{Haar}}$ , then it is distorted by application of  $\rho^{1/2}$ , finally it is normalized. This prescription returns the Haar measure itself when  $\rho = \mathbb{I}_A/d_A$  i.e. when  $\beta = 0$ , but when  $\beta > 0$  it biases the distribution toward lower-energy states, so that the mean state (first moment) is  $\rho$ . The Scrooge ensemble with  $\rho = \text{Tr}_B(e^{-\beta H})$  (at the appropriate temperature) was found to describe the limiting projected ensembles formed from Hamiltonian eigenstates as well as Hamiltonian quench dynamics at late times, again in the case of energy non-revealing measurements [8]. Interestingly, out of all state ensembles with the same first moment  $\rho$  (in this case the canonical density matrix), the Scrooge ensemble is the one that minimizes a quantum information property called “accessible information” [45] — the maximal amount of classical information extractable from the ensemble of quantum states. This is in line with the intuition that a complex, scrambling bath hides information of a local subsystem and makes it maximally difficult to extract [14, 15].

Moving to the generic case of energy-revealing measurements gives an even richer phenomenology. As we have discussed [and as sketched in Fig. 2(b)], in this case a measurement outcome on  $B$  may reveal an above- or below-average amount of energy in the bath, which will have to be compensated by an opposite energy fluctuation in the system, systematically biasing the post-measurement state toward high- or low-energy parts of the Hilbert space. Thus, instead of a unique Scrooge ensemble specified only by the global temperature, Ref. [14] identified a composite ensemble, dubbed the ‘generalized Scrooge ensemble’ (GSE), where each possible measurement outcome on the bath yields a state on the system drawn from a *different* Scrooge ensemble, each of which harbors an average energy consistent with the difference between the conserved total energy and the inferred energy from the measurement outcome. Notably, the limiting ensemble in this energy-conserving scenario in principle contains an exponential amount of data: each of the  $2^{N_B}$  possible measurement outcomes on  $B$  yields different information about the subsystem  $A$ ’s energy and defines a different Scrooge ensemble, which enters into the construction of the GSE.

Our work uncovers closely related phenomenology in

$U(1)$ -symmetric systems, including the strong dependence on the choice of measurement basis (from ‘non-revealing’ to ‘maximally-revealing’) and the emergence of Scrooge and generalized Scrooge ensembles. However, there are also different aspects that appear to be intrinsic to the  $U(1)$  case as opposed to the Hamiltonian case: for instance the GSE is found to depend only on a polynomial (in fact,  $O(N)$ ) amount of data, with a more transparent physical meaning related to the charge fluctuations in the initial state.

### III. PROJECTED ENSEMBLE OF A RANDOM $U(1)$ -SYMMETRIC STATE

To begin, we consider the conceptually cleanest scenario: the projected ensemble of a global Haar random state with definite charge  $Q_0$ , generated from computational ( $z$ ) basis, maximally charge-revealing measurements on  $B$ . Despite its relative simplicity, this scenario is of great practical interest; in fact, it is the only allowed case when the symmetry is a symmetry of the universe (e.g., the  $U(1)$  of electromagnetism) and not just of the system under consideration. In that case, superselection rules forbid charge fluctuations in the (pure) initial state as well as in the measurement basis. We have adopted a convention where without loss of generality the charge  $Q_0$  assumes values from 0 to  $N$  (this can be achieved with a suitable global shift in the measurement values; for example, the local magnetization  $M = \sum_{i=1}^N Z_i$  is related to  $Q_0$  via  $Q_0 = M + N/2$ ).

In this setting, complications due to fluctuations of charge in the initial state do not arise. Further, the nature of the measurements is such that upon observing a bit-string  $z$  which carries charge  $Q_B$ , the projected state is guaranteed to have charge  $Q_A = Q_0 - Q_B$ . Repeating this process many times, it should be expected that states from any *fixed* charge sector  $Q_A$  should be sampled uniformly; then, how often a state with charge  $Q_A$  is sampled relative to a state with charge  $Q'_A$  should be set by the ratio of the sizes of the charge sectors. Indeed, we have:

**Theorem 1** *Let  $|\Psi\rangle$  be a Haar random state on  $N$  qubits with definite charge  $Q_0$ , so that the charge density is  $\sigma \equiv Q_0/N \in [0, 1]$  and the state lives in a Hilbert space with dimension  $d_{Q_0} = \binom{N}{Q_0}$ . Construct the projected ensemble  $\mathcal{E}_A$  on  $N_A$  qubits, using measurements of  $B$  in the computational ( $z$ ) basis. Then as long as*

$$N_B H(\sigma) = \Omega(k N_A + \log(\epsilon^{-1}) + \log \log(\delta^{-1})) \quad (10)$$

where  $H(\sigma) = -\sigma \log \sigma - (1 - \sigma) \log(1 - \sigma)$  is the binary entropy, with probability at least  $1 - \delta$  the  $k$ -th moment of the projected ensemble obeys

$$\frac{1}{2} \|\rho^{(k)} - \rho_{DS, Q_0}^{(k)}\|_{tr} \leq \epsilon, \quad (11)$$

<sup>1</sup> A physical way of implementing this sampling is to apply the POVM  $\{d_A |\psi\rangle\langle\psi| : \psi \sim \text{Haar}\}$  to the state  $\rho$ ; this POVM corresponds to a projective measurement in a Haar-random basis. The measurement outcome  $|\psi\rangle\langle\psi|$  has the desired distribution.

where  $\rho_{DS,Q_0}^{(k)}$  is the  $k$ -th moment of the ‘direct sum (DS)’ ensemble,

$$\rho_{DS,Q_0}^{(k)} = \bigoplus_{Q_A=0}^{N_A} \pi(Q_A|Q_0) \rho_{Haar,A,Q_A}^{(k)}. \quad (12)$$

Above,  $\rho_{Haar,A,Q_A}^{(k)}$  is the  $k$ -th moment of the Haar ensemble on states on  $A$  with fixed charge  $Q_A$ ,  $d_{Q_A} = \binom{N_A}{Q_A}$  is the dimension of charge sector  $Q_A$  on  $N_A$  qubits, and the probability  $\pi(Q_A|Q_0) = d_{Q_A} d_{Q_B} / d_{Q_0}$ , where  $d_{Q_B} = \binom{N-N_A}{Q_0-Q_A}$ .

Theorem 1 in fact yields more than just the aforementioned expected outcome: it states that, with high probability, a *single instance* of a charge-symmetric Haar random state of a large enough system will generate a projected ensemble very close to the ‘direct sum’ ensemble. The latter consists of a direct sum of Haar random distributions within each charge sector  $Q_A$ , weighted by the frequency  $\pi(Q_A|Q_0)$  with which  $Q_A$  appears — a purely entropic factor. Our Theorem 1 can be understood as the analog of Theorem 1 of Ref. [8].

The proof of this theorem is technical but straightforward, and left to Appendix A. We quickly sketch the logic here: first, we show that on average over input states  $|\Psi\rangle$ , the projected ensemble is the direct sum ensemble. Second, we show that the projected ensemble is Lifshitz continuous, and thus (by Levy’s lemma [48]) it concentrates around this expected value with high probability in the limit of large bath size.

Thus, we see from this simple example the role of symmetries in endowing the limiting projected ensemble of a random symmetric state with more structure than just a featureless Haar distribution over the full Hilbert space: the system becomes Haar random within individual charge sectors. However, the fact that the direct sum ensemble should emerge in this case is to be expected, and a more interesting question arises when considering initial states with non-definite charge, as well as general measurement bases, as described in Sec. II.

#### IV. THEORY OF UNIVERSAL LIMITING ENSEMBLES FOR GENERAL INITIAL STATES AND MEASUREMENT BASES

Having addressed the case of a symmetric initial state subject to  $z$ -basis measurements, we now move on to the general case. From this point forward, we implicitly assume the  $U(1)$  symmetry does not obey a superselection rule, so coherent superpositions of different charge sectors are allowed. Since the rigorous proof techniques utilizing random matrix theory in Sec. III do not straightforwardly extend to this more general case, we will adopt a different approach to make analytical progress. We describe the main conceptual steps involved in this theory below, relegating the technical details to App. B. The results are also summarized in Table I.

Let us be given a general initial state  $|\Psi\rangle$  on  $N$  qubits. We can always decompose it into charge sectors as

$$|\Psi(0)\rangle = \sum_{Q=0}^N \sqrt{p(Q)} |\Phi_Q\rangle, \quad (13)$$

where  $p(Q) = \langle \Psi(0) | \hat{\Pi}_Q | \Psi(0) \rangle$  is the charge probability distribution of the initial state,  $\hat{\Pi}_Q$  is the projector on charge sector  $Q$ , and  $|\Phi_Q\rangle$  is a normalized state supported in charge sector  $Q$ .

Our goal is to understand, given a model of  $U(1)$ -symmetric chaotic quantum dynamics (e.g. in Sec. V we will specialize to local random circuits of  $U(1)$ -symmetric gates for numerical simulations), the late-time form of the projected ensemble constructed from such a state. While  $p(Q)$  is a constant of the dynamics, the states  $\{|\Phi_Q\rangle\}_Q$  will change as a function of time. We expect that *each of these charge-definite states, over long times, will independently explore their individually available Hilbert spaces*. We note that this assumption (a version of ‘‘complete Hilbert space ergodicity’’ [49, 50]) is not trivial—indeed, it was shown that the entire  $U(1)$ -symmetric unitary group cannot be generated from *local*  $U(1)$ -symmetric interactions [51]. However, we show in App. C that this does not limit the set of states that can be reached from a given initial state.

Therefore, under the aforementioned assumptions, our theory posits that the late time limit of the projected ensemble should be invariant under Haar-averaging the  $\{|\Phi_Q\rangle\}_Q$  states over their respective charge sectors:

$$\rho_{\mathcal{E}}^{(k)} \xrightarrow{t \rightarrow \infty} \mathbb{E}_{\{\Phi_Q \sim \text{Haar}(\mathcal{H}_Q)\}} \sum_b \frac{(\langle b | \Psi_{p,\Phi} \rangle \langle \Psi_{p,\Phi} | b \rangle)^{\otimes k}}{(\langle \Psi_{p,\Phi} | b \rangle \langle b | \Psi_{p,\Phi} \rangle)^{k-1}}, \quad (14)$$

with  $|\Psi_{p,\Phi}\rangle = \sum_Q \sqrt{p(Q)} |\Phi_Q\rangle$ , a linear superposition of random states with charge  $Q$ , with relative weights set by  $p(Q)$  defined by the initial state. Here  $b$  denotes the measurement outcome in some measurement basis  $M$  (we have relaxed the assumption of measurement in the computational basis to local projective measurements along some common but arbitrary axis).

Eq. (14) describes an ensemble that depends solely on the charge distribution  $p(Q)$  of the initial state. All other information about the initial state has been lost. This resembles how the standard thermodynamic Gibbs state depends on the average charge  $\langle \hat{Q} \rangle = \sum_Q p(Q) Q$  (through the chemical potential). In this case, however, it is *a priori* possible for higher moments of the charge distribution, and in fact for the distribution as a whole, to determine the limiting ensemble. This illustrates how familiar concepts in standard thermalization can be non-trivially generalized in deep thermalization.

While Eq. (14) is a prediction for the limiting form of the projected ensemble in dynamics with symmetries (it has eliminated the need to solve for the microscopic dynamics), it is not fully satisfactory: it still involves a sum over the exponentially many measurement outcomes, and hence a further simplification exposing the

Initial state's charge distribution	Measurement basis	
	Maximally charge-revealing ( $z$ )	Charge non-revealing ( $x$ - $y$ plane)
No fluctuations, $Q = N/2$	'Direct sum' ensemble (Sec. III, IV A 1)	Haar ensemble (Sec. IV B)
No fluctuations, $Q \neq N/2$		Scrooge ensemble (Sec. IV B)
Equilibrium, $\beta\mu = 0$	Haar ensemble (Sec. IV A 2)	Haar ensemble ( <i>numerical</i> , Sec. V B)
Equilibrium, $\beta\mu \neq 0$	Scrooge ensemble (Sec. IV A 2)	?
General	Generalized Scrooge ensemble (Sec. IV A)	

Table I. Summary of the results of Sec. IV: limiting form of the projected ensemble as a function of the charge fluctuations in the initial state and the choice of measurement basis on the bath. We additionally include the rigorous result of Sec. III and a numerical result from Sec. V for which we have no corresponding analytical statement (all other numerical results are in agreement with predictions). The entries marked by a '?' in the table are not addressed in this work.

core of this object is desirable. In general, a direct evaluation of Eq. (14) is challenging. However, much progress can be made under the physically relevant scenarios of measurements in a basis which fully reveals charge information ( $b = z$ -basis) and also a basis which never reveals charge information ( $b = x, y$ -basis) — the two scenarios sketched in Fig. 2. Further, to deal with the technical difficulty of averaging the integrands which contain  $\{|\Phi_Q\rangle\}$  in the denominator, it is possible to carry out the calculation by means of a 'replica trick', where one treats the power  $1 - k \equiv n$  of the denominator as a positive integer, carries out the Haar averages by well established Weingarten calculus methods [16], and finally takes the 'replica limit'  $n \rightarrow 1 - k$ . This method is not mathematically rigorous but is widely applied in statistical physics and often yields correct answers in practice. Nonetheless, the answers should be checked by independent methods. In this work we will benchmark the results against exact numerical calculations (in Sec. V) and against the rigorous result of Sec. III.

### A. Maximally charge-revealing measurements

We first focus on the case of measurements in the computational ( $z$ ) basis. These measurements fully reveal the local charge density (0 or 1) at each measured site, and thus are 'maximally charge-revealing' [see Sec. II B 2, and Fig. 2(b)]. Our result in Sec. III on a Haar-random state of fixed charge subjected to  $z$ -basis measurements already constitutes an extreme example of the effect of such measurements — since the global charge  $p(Q) = \delta_{Q, Q_0}$  is sharply defined, any measurement outcome on  $B$  completely determines the charge on  $A$ ,  $Q_A = Q_0 - Q_B$ , so the projected ensemble acquires a direct-sum structure across charge sectors. Now we aim to generalize that result from the case of a deterministic total charge to a general probability distribution of charge  $p(Q)$  in the initial state. In this case, the measurement outcome on  $B$  may increase our knowledge of the charge on  $A$ , but will not completely determine it in general.

We carry out the replica calculation for this case in Appendix B. Even within the 'replica trick', the problem is not analytically solvable; another limit is needed:

the limit of large Hilbert space dimension for the charge sectors of the whole system,  $\binom{N}{Q}$ , and of the subsystem  $A$ ,  $\binom{N_A}{Q_A}$ . The result is therefore expected to be accurate only in the limit of a large subsystem,  $N_A \rightarrow \infty$ , which is a stronger requirement than just the thermodynamic limit  $N \rightarrow \infty$ . Within this approximation, the result of our calculation is in the form of a generalized Scrooge ensemble (GSE) [14].

The GSE, introduced in Ref. [14] to describe the projected ensemble of chaotic Hamiltonian systems at late times under general 'energy-revealing' measurements, is defined as a stochastic mixture of Scrooge ensembles [the Scrooge ensemble is reviewed in Sec. II B 2, see Eq. (9)]. Given a probability distribution over density matrices  $\{p_i, \rho_i\}$ , we can define a new ensemble, the GSE, by the following two-step prescription: (i) draw a density matrix  $\rho_i \sim p_i$ ; then (ii) draw a state  $|\psi\rangle$  from  $\mathcal{E}_{\text{Scrooge}}[\rho_i]$ . It is easy to see that the  $k$ -th moment operator of a GSE reads

$$\rho_{\text{GSE}}^{(k)} = \sum_i p_i \rho_{\text{Scrooge}}^{(k)}[\rho_i], \quad (15)$$

where  $\rho_{\text{Scrooge}}^{(k)}[\rho]$  is the  $k$ -th moment of the Scrooge ensemble for density matrix  $\rho$ .

The result of our calculation in Appendix B 3 states that the limiting form of the projected ensemble at late times is a GSE:

$$\rho_{\mathcal{E}}^{(k)} \xrightarrow{t \rightarrow \infty} \sum_{Q_B=0}^{N_B} \pi_p(Q_B) \rho_{\text{Scrooge}}^{(k)}[\bar{\rho}_{A,p}(Q_B)], \quad (16)$$

where  $\pi_p$  is a probability distribution of charge on  $B$  and  $\{\bar{\rho}_{A,p}(Q_B)\}_{Q_B}$  is a family of density matrices on  $A$  depending on  $Q_B$ . Both objects depend on the charge distribution  $p(Q)$  of the initial state. The probability distribution  $\pi_p$  is given by

$$\pi_p(Q_B) = \sum_{Q=0}^N \pi(Q_B|Q) p(Q), \quad (17)$$

$$\pi(Q_B|Q) = \binom{N_A}{Q_A} \binom{N_B}{Q_B} \binom{N}{Q}^{-1}; \quad (18)$$



here  $\pi(Q_B|Q)$  represents the probability of measuring charge  $Q_B$  on  $B$  (and  $Q_A = Q - Q_B$  on  $A$ ) given that the initial state had total charge  $Q$ , on average over random charge-conserving dynamics at long times. This is a purely combinatorial factor. The density matrices  $\{\bar{\rho}_{A,p}(Q_B)\}_{Q_B}$  are given by

$$\bar{\rho}_{A,p}(Q_B) = \sum_{Q_A=0}^{N_A} \frac{\hat{\Pi}_{Q_A}}{\text{Tr}(\hat{\Pi}_{Q_A})} \pi_p(Q_A + Q_B|Q_B), \quad (19)$$

where the conditional probability  $\pi_p(Q_A + Q_B|Q_B)$  is given by Bayes' theorem:

$$\pi_p(Q|Q_B) = \frac{\pi(Q_B|Q)p(Q)}{\pi_p(Q_B)}. \quad (20)$$

This defines a ‘posterior’ distribution,  $Q_A \sim \pi_p(Q_A + Q_B|Q_B)$ , as in Fig. 2 (there we dropped the  $Q_B$  in the first argument to lighten the notation).

Physically, the GSE prescription in Eq. (16) can be interpreted as a distribution of states constructed as follows:

- (i) We first draw a value of the charge  $Q_B$  on the bath according to the distribution  $\pi_p(Q_B)$ , Eq. (17), which is the distribution of charge on  $B$  assuming that the overall charge  $Q \sim p(Q)$  of the system is completely scrambled.
- (ii) Knowledge about  $Q_B$  from (i) gives us some information about the charge on  $A$ : we then update our belief about the charge on  $A$  to the posterior distribution  $\pi_p(Q_A + Q_B|Q_B)$ , Eq. (20).
- (iii) Lastly we sample a state from the Scrooge ensemble  $\mathcal{E}_{\text{Scrooge}}[\bar{\rho}_{A,p}(Q_B)]$  on  $A$ , with the density matrix  $\bar{\rho}_{A,p}(Q_B)$  [Eq. (19)] reflecting our updated belief.

Two notable limiting cases for this ensemble are discussed next.

### 1. No charge fluctuations

As a sanity check of our predictions, we apply our theory to the case considered in Sec. III when the initial state has a well defined charge,  $p(Q) = \delta_{Q,Q_0}$ . Then it is straightforward to see that

$$\pi_p(Q_A + Q_B|Q_B) = \delta_{Q_A+Q_B,Q_0} \quad (21)$$

(i.e., since we are already certain about  $Q = Q_0$ , drawing  $Q_B$  tells us with certainty that  $Q_A = Q_0 - Q_B$ ) and thus the average state on  $A$  upon measuring bit-strings on  $B$  with charge  $Q_B$  is

$$\bar{\rho}_{A,p}(Q_B) = \frac{\hat{\Pi}_{Q_0-Q_B}}{\text{Tr}(\hat{\Pi}_{Q_0-Q_B})} = \frac{\hat{\Pi}_{Q_A}}{\text{Tr}(\hat{\Pi}_{Q_A})}, \quad (22)$$

i.e., a maximally mixed state of fixed charge. The Scrooge ensemble  $\mathcal{E}_{\text{Scrooge}}[\bar{\rho}_{A,p}(Q_B)]$  is hence simply the

Haar measure on the charge sector  $Q_A = Q_0 - Q_B$ . The GSE then returns the direct sum of Haar measures across charge sectors weighted according to  $\pi_p(Q_B) = \pi(Q_B|Q_0)$ , in agreement with the rigorous results of Sec. III.

### 2. Equilibrium charge fluctuations

Another case where the GSE reduces to a simple form is when the initial state has the same charge distribution as a thermal equilibrium state,

$$\rho_{\text{eq.}} = \frac{e^{\beta\mu\hat{Q}}}{(1 + e^{\beta\mu})^N}. \quad (23)$$

Here,  $\beta$  is the inverse temperature and  $\mu$  the chemical potential. Together, they make up the fugacity  $z = e^{\beta\mu}$ . A pure initial state with this charge distribution is, for instance,  $(|0\rangle + e^{\beta\mu}|1\rangle)^{\otimes N}$ , up to normalization. One has in this case

$$p(Q) = \text{Tr} \left( \hat{\Pi}_Q \frac{z^{\hat{Q}}}{(1+z)^N} \right) = \frac{z^Q}{(1+z)^N} \binom{N}{Q}. \quad (24)$$

It is straightforward to derive the probability distribution of charge on  $B$ , Eq. (17),

$$\pi_p(Q_B) = \sum_{Q_A} \frac{z^{Q_A+Q_B}}{(1+z)^{N_A+N_B}} \binom{N_A}{Q_A} \binom{N_B}{Q_B} \quad (25)$$

$$= \frac{z^{Q_B}}{(1+z)^{N_B}} \binom{N_B}{Q_B}, \quad (26)$$

and the post-measurement conditional distribution of charge on  $A$ , Eq. (20),

$$\pi_p(Q_A + Q_B|Q_B) = \frac{z^{Q_A}}{(1+z)^{N_A}} \binom{N_A}{Q_A}. \quad (27)$$

Both of these have the same form of a thermal equilibrium charge distribution with the same value of  $z = e^{\beta\mu}$ . Qualitatively, this means that  $Q_A$  and  $Q_B$  separately follow (uncorrelated) thermal equilibrium distributions, and measuring  $Q_B$  does not give us any information about  $Q_A$ .

It follows that the density matrices used in the GSE construction, Eq. (19), are given by

$$\begin{aligned} \bar{\rho}_{A,p}(Q_B) &= \sum_{Q_A=0}^{N_A} \frac{z^{Q_A}}{(1+z)^{N_A}} \binom{N_A}{Q_A} \frac{\hat{\Pi}_{Q_A}}{\text{Tr}(\hat{\Pi}_{Q_A})} \\ &= \sum_{Q_A=0}^{N_A} \hat{\Pi}_{Q_A} \frac{z^{Q_A}}{(1+z)^{N_A}} \propto e^{\beta\mu\hat{Q}_A}, \end{aligned} \quad (28)$$

where we used the fact that  $\text{Tr}(\hat{\Pi}_{Q_A}) = \binom{N_A}{Q_A}$ . Since all the density matrices  $\{\bar{\rho}_{A,p}(Q_B)\}$  are equal, independent of  $Q_B$ , the GSE in this case reduces to the simple Scrooge ensemble induced by the thermal equilibrium

state  $e^{\beta\mu\hat{Q}_A}$ . In the special case of infinite temperature (or zero chemical potential,  $\beta\mu = 0$ ), the Scrooge ensemble further reduces to the Haar ensemble over the entire Hilbert space of  $A$ . We comment further on the significance of this result in relation to ‘charge-non-revealing’ measurements below.

### B. Charge-non-revealing measurements

We next consider measurements in the Pauli  $x$  basis (or in fact any vector in the  $x$ - $y$  plane) which do not reveal any information about the local charge density. As we reviewed in Sec. II B 2 [see also Fig. 2(b)], Ref. [8] found that the projected ensemble under Hamiltonian dynamics and ‘energy-non-revealing’ measurements is well described by a single (i.e., not generalized) Scrooge ensemble; it is reasonable to expect similar behavior under the  $U(1)$  on-site symmetry. In Appendix B 4 we show that this is indeed the case when starting from states of a well-defined, but arbitrary, charge  $Q_0$ .

Specifically, we find that in the limit of large system and subsystem size,  $N_A, N_B \gg 1$ , the limiting ensemble is predicted to take the form  $\mathcal{E}_{\text{Scrooge}}[\bar{\rho}_A(Q_0)]$  determined by the density matrix

$$\begin{aligned} \bar{\rho}_A(Q_0) &= \sum_{Q_A=0}^{N_A} \binom{N_B}{Q_0 - Q_A} \binom{N}{Q_0}^{-1} \hat{\Pi}_{Q_A} \\ &= \sum_{Q_A=0}^{N_A} \pi(Q_A|Q_0) \frac{\hat{\Pi}_{Q_A}}{\text{Tr}(\hat{\Pi}_{Q_A})}. \end{aligned} \quad (29)$$

In the second line we have written the density matrix explicitly as a stochastic mixture of maximally-mixed states in the charge sectors, weighted by the probability distribution  $\pi(Q_A|Q_0) = \binom{N_A}{Q_A} \binom{N_B}{Q_0 - Q_A} \binom{N}{Q_0}^{-1}$ . This is a purely combinatorial factor representing the probability of finding charge  $Q_A$  in subsystem  $A$  on average over all initial states of total charge  $Q_0$ . Notably, for a charge-neutral initial state ( $Q_0 = N/2$ ), the density matrix  $\bar{\rho}_A(Q_0)$  in Eq. (29) becomes close to the identity, up to corrections of order  $N_A/N$  which vanish in the thermodynamic limit, so the Scrooge ensemble reduces to the Haar ensemble in that case.

The fact that we obtain a single Scrooge ensemble rather than a GSE may be understood as a consequence of the fact that  $x$ -basis measurement outcomes on  $B$  do not provide any information on the way that the charge  $Q_0$  is partitioned between  $A$  and  $B$ . The Scrooge ensemble is thus completely determined by the *prior* distribution  $\pi(Q_A|Q_0)$ . This should be contrasted to the case of charge-revealing measurements, where the measured value of  $Q_B$  generically updates our belief about the charge in  $A$ , giving rise to a GSE—a different Scrooge ensemble for each possible outcome  $Q_B$ . An exception is the case studied in Sec. IV A 2, of states with an equilibrium charge distribution. In that case, since the charge distri-

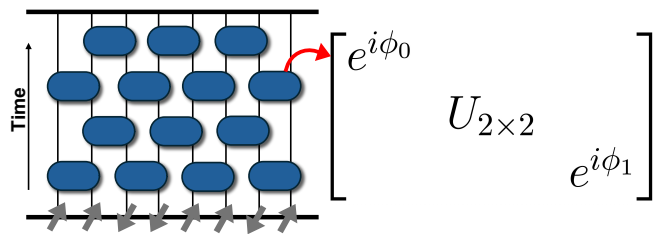


Figure 3. Left: a random  $U(1)$ -symmetric quantum circuit acting on a 1D qubit chain, the setting of our numerical simulations. Right: implementation of the  $U(1)$  symmetry (charge conservation) in the circuit. Each two-qubit quantum gate has a block-diagonal form such that the weights on the one-dimensional charge sectors  $\{|00\rangle\}$ ,  $\{|11\rangle\}$  are preserved but are imparted random phases  $e^{i\phi_0}$ ,  $e^{i\phi_1}$ , while the two-dimensional charge sector  $\{|01\rangle, |10\rangle\}$  is Haar randomized by a two-by-two Haar random unitary  $U_{2 \times 2}$ .

butions on  $A$  and  $B$  are fully uncorrelated, *all measurement bases are effectively ‘charge-non-revealing’*—even the  $z$  basis. Remarkably the result of Sec. IV A 2 (a single Scrooge ensemble) is in agreement with the present result for  $x$ -basis measurements, showing a universality of deep thermalization across different instances of ‘charge-non-revealing’ measurements.

### C. Partially charge-revealing measurements

The analyses above focused on the cases of measurement bases which (i) fully reveal charge information ( $z$ -basis), or (ii) never reveal charge information ( $x$ - $y$  plane basis). These already yielded very rich physics. A natural question is to inquire about measurement bases which *partially* reveal charge information, such as in a mixed  $x$ - $z$  basis. In this case, we may conjecture a limiting distribution given by a yet more generalized (and complicated) Scrooge ensemble, arising from a similar construction to the GSE of Eq. (16) but differing in that a different Scrooge ensemble should be sampled for each given bitstring measurement outcome. This is similar to the case of energy-conserving dynamics [14], but is in contrast to the GSE of Eq. (16) where only the charge information of the bitstring determines the Scrooge ensemble to be sampled from. We leave such interesting further directions for future work.

## V. NUMERICAL RESULTS

In this section we present data from numerical simulations to corroborate our analytical predictions of Sec. IV. We focus on 1D qubit chains that evolve under random unitary circuits of two-qubit gates applied to the system in a staggered (‘brickwork’) pattern, as shown in Fig. 3. We impose a local  $U(1)$  symmetry tied to the conservation of the  $z$  component of the total spin,

$\hat{Q} = \sum_i (\mathbb{I} + Z_i)/2$ , by restricting the gates in the random unitary circuits to have a block-diagonal form, also shown in Fig. 3. Specifically the states  $|00\rangle, |11\rangle$  span one-dimensional charge sectors and thus a local gate simply imparts uniformly random phases  $e^{i\phi_0}, e^{i\phi_1}$  onto them ( $\phi_0$  can be set to zero by fixing the overall phase), while the states  $|01\rangle, |10\rangle$  span a two-dimensional charge sector and transform within themselves via the action of a Haar random unitary in  $U(2)$ . This model has been used to study the dynamics of generic chaotic systems with a local conserved density in an analytically tractable way [21–23].

To test the analytical predictions from Sec. IV, we aim to numerically characterize the projected ensemble of a time-evolved state  $|\Psi(t)\rangle = U_t U_{t-1} \cdots U_1 |\Psi(0)\rangle$  in the limit  $t \rightarrow \infty$ , where  $\{U_t\}$  is a sequence of brickwork layers of unitary gates sampled randomly as described above, and  $|\Psi(0)\rangle$  is an arbitrary initial state of the qubit chain. For concreteness we consider the following family of initial states, parametrized by an angle  $\theta \in [0, \pi/2)$ :

$$|\Psi(0)\rangle = [(\cos \theta |0\rangle + \sin \theta |1\rangle) \otimes (\sin \theta |0\rangle + \cos \theta |1\rangle)]^{\otimes \frac{N}{2}} \quad (30)$$

(the total number of qubits  $N$  is taken to be even). These are product states with average charge  $\langle \hat{Q} \rangle = \langle \Psi(0) | \hat{Q} | \Psi(0) \rangle = N/2$  for all  $\theta$ . This is the same average charge as the maximally mixed state,  $\langle \hat{Q} \rangle = \text{Tr}(\hat{Q})/\text{Tr}(\mathbb{I}) = N/2$ , i.e. the state is at charge neutrality. However, as a function of  $\theta$ , the states have different fluctuations of the charge: for example, the variance of  $Q$  is given by

$$\langle \Psi(0) | \hat{Q}^2 | \Psi(0) \rangle - \langle \Psi(0) | \hat{Q} | \Psi(0) \rangle^2 = \frac{N}{4} \sin^2(2\theta). \quad (31)$$

This family of states covers several limiting cases of interest, discussed in the general theory of Sec. IV. For  $\theta = 0$  we have  $|\Psi(0)\rangle = |01\rangle^{\otimes N/2}$ , known as the Néel state in the context of magnetism; this state has no charge fluctuations at all,  $p(Q) = \delta_{Q, N/2}$ . For  $\theta = \pi/4$  we have  $|\Psi(0)\rangle = |+\rangle^{\otimes N}$ , which has  $p(Q) = 2^{-N} \binom{N}{Q}$ , the same distribution as a maximally mixed state. We study ‘maximally charge-revealing’ ( $z$  basis) measurements in Sec. VA and ‘charge-non-revealing’ ( $x$  basis) measurements in Sec. VB.

## A. Maximally charge-revealing measurements

### 1. No charge fluctuations: Néel state

For  $\theta = 0$  we recover the Néel state,  $|01\rangle^{\otimes (N/2)}$ , which is a state of definite total charge  $Q_0 = N/2$ . Since the measurements are carried out in the  $Z$  basis, each projected state must then have a definite charge, too:  $Q_A = Q_0 - Q_B$ , where  $Q_B$  is the charge on  $B$  revealed by the measurement. As we have discussed in Sec. IV A 1,

the form of the projected ensemble in this case is predicted to be a direct sum of Haar ensembles in each charge sector:

$$\rho_{\text{target}}^{(k)} = \rho_{\text{DS}, Q_0}^{(k)} = \bigoplus_{Q_A=0}^{N_A} \pi(Q_A | Q_0) \rho_{\text{Haar}, A, Q_A}^{(k)}, \quad (32)$$

with  $\pi(Q_A | Q_0) = \binom{N_A}{Q_A} \binom{N_B}{Q_0 - Q_A} \binom{N}{Q_0}^{-1}$  and, for the Néel state,  $Q_0 = N/2$ . Here  $\rho_{\text{Haar}, A, Q_A}^{(k)}$  is the  $k^{\text{th}}$  moment of the Haar ensemble in the Hilbert space of charge sector  $Q_A$ .

We test the prediction of Eq. (32) by calculating the trace distance  $\Delta^{(k)}$  between the  $k$ -th moment operators, defined in Eq. (8). For simplicity, we fix the size of the subsystem  $A$  to  $N_A = 2$  (the minimal subsystem with a nontrivial charge sector,  $Q_A = 1$ ) and the statistical moment to  $k = 2$ . We vary the total size of the system  $N$  between 8 and 24 qubits to investigate the scaling toward the thermodynamic limit  $N \rightarrow \infty$  as the subsystem  $A$  is kept fixed. We average the distance measure  $\Delta^{(2)}$  over 128 realizations of the random circuit. Note that the average takes place *after* the calculation of the (non-linear) distance measure  $\Delta^{(2)}$ , so the emergence of universal random wavefunction distributions (in this case, the ‘direct sum’ ensemble) is due to the randomness inherent in the projected ensemble, not to the randomness of the circuit realization.

As shown in Fig. 4, the trace distance  $\Delta^{(2)}$  decays with time until it reaches a plateau arising from the finite-sized nature of the simulation. As the total system size  $N$  increases, this plateau decays exponentially with the total system size  $N$ , as shown in the inset of Fig. 4. An exponential fit yields  $2^{-0.48N}$ , consistent with the inverse square root of the total Hilbert space dimension  $d = 2^N$ . This scaling agrees with the expected local fluctuations in a Haar-random state of  $N$  qubits, as the inverse square root of the Hilbert space dimension [8]. This suggests  $\Delta^{(2)} \rightarrow 0$  in the limit of large system size  $N$  and long time  $t$ , which signifies deep thermalization to the ‘direct sum’ form of the projected ensemble, Eq. (32), at the level of the second moment  $k = 2$ . These observations are in agreement with our theoretical predictions, including Theorem 1.

### 2. Equilibrium charge fluctuations: $X$ -basis state

For  $\theta = \pi/4$  we have the initial state  $|+\rangle^{\otimes N}$ , whose charge distribution is the same as that of the maximally mixed state. We have seen in Sec. IV A 2 that in this case the limiting form of the projected ensemble should be Haar-random in the full Hilbert space. To test if and how the projected ensemble approaches the Haar ensemble over time, we repeat the calculation of Eq. (8) as we did for the Néel state above, but using the Haar ensemble as target.

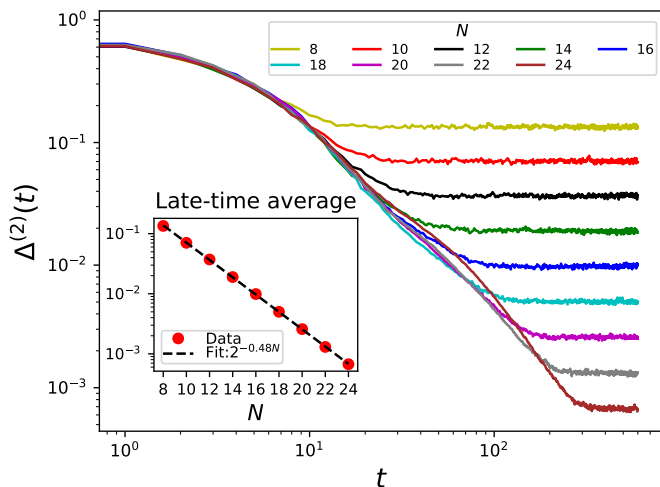


Figure 4. Trace distance  $\Delta^{(2)}$  between the second moment of the projected ensemble and that of the ‘direct sum’ target ensemble Eq. (32) as a function of time, for the initial state  $|01\rangle^{\otimes N/2}$  and measurements in the  $z$  basis. The total system size  $N$  is varied while the subsystem size  $N_A$  is fixed to 2. Results are averaged over 128 realizations of the random circuit. Inset: late-time averaged value of  $\Delta^{(2)}$  as a function of  $N$ . Exponential fit (dashed line) yields  $2^{-0.48N}$ , consistent with the expected  $2^{-N/2}$ .

As shown in Fig. 5, the distance  $\Delta^{(2)}$  between second moment operators decays with time until it eventually saturates to a non-zero plateau arising due to finite-size effects. The value of this late-time plateau decays exponentially in  $N$ , as shown in the inset of Fig. 5. An exponential fit of the late-time average values vs  $N$  yields the scaling  $\sim 2^{-0.50N}$ , again consistent with  $1/\sqrt{d_A}$ . We can infer that the distance  $\Delta^{(2)}$  approaches zero in the thermodynamic limit  $N \rightarrow \infty$  (with fixed  $N_A$ ), which is consistent with our predictions of deep thermalization to the Haar ensemble.

### 3. General initial states

So far we have discussed the two extreme cases of maximal and minimal information about the charge in the initial state:  $\theta = 0$  (Néel state) and  $\theta = \pi/4$  ( $x$ -basis state). The target ensembles for these two cases reduce to simple forms—respectively the Haar ensemble and the direct sum of charge-sector Haar ensembles. For intermediate values of  $\theta$ , the predicted limiting form of the projected ensemble becomes more complex and is given by the GSE, Eq. (16). To test this prediction, we select an intermediate value of  $\theta = \pi/20$  (the reason for this parameter choice is that the GSE’s second-moment operator is roughly equidistant from those at  $\theta = 0$  and  $\theta = \pi/4$ , as discussed in Appendix D). We numerically construct the GSE’s second moment operator by Monte Carlo sampling  $M$  pairs  $(Q_B, |\psi\rangle)$ , where  $Q_B \sim \pi_p(Q_B)$

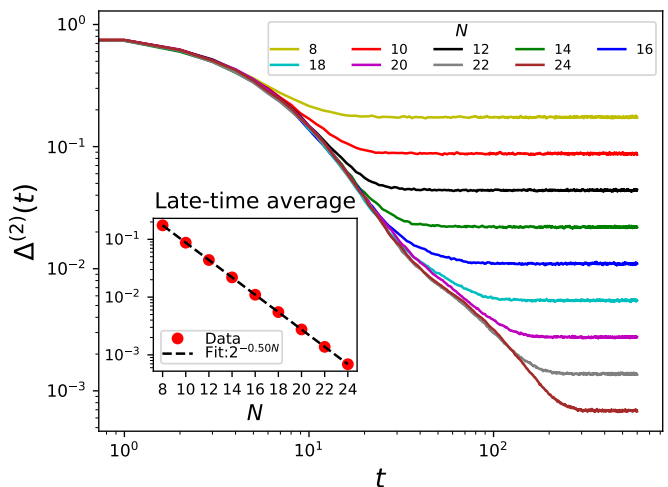


Figure 5. Trace distance  $\Delta^{(2)}$  between the second moment of the projected ensemble and that of the Haar ensemble over the entire Hilbert space as a function of time, for the initial state  $|+\rangle^{\otimes N}$  and measurements in the  $z$  basis. The total system size  $N$  is varied while the subsystem size  $N_A$  is fixed to 2. Results are averaged over 128 realizations of the random circuit. Inset: late-time averaged value of  $\Delta^{(2)}$  as a function of  $N$ . The behavior is consistent with  $2^{-N/2}$  (dashed line), indicating convergence to  $\Delta^{(2)} = 0$  in the thermodynamic limit.

and  $|\psi\rangle \sim \mathcal{E}_{\text{Scrooge}}[\bar{\rho}_{A,p}(Q_B)]$ , and setting

$$\rho_{GSE}^{(2)} \simeq \frac{1}{M} \sum_{i=1}^M |\psi_i\rangle\langle\psi_i|^{\otimes 2}. \quad (33)$$

We find this approximation is numerically converged to the required precision at the largest system size studied ( $N_A = 4$ ,  $N = 24$ ) with  $M = 10^8$  samples, see Appendix D. Finally, we numerically compute the trace distance  $\Delta^{(2)}$  between the second moment of the projected ensemble and that of the GSE, Eq. (33).

Our derivation of the GSE, Appendix B3, relies on an assumption of large Hilbert space dimension not only for the whole system ( $N \rightarrow \infty$ ), but also for the subsystem of interest ( $N_A \rightarrow \infty$ ). To study the possible dependence on subsystem size, we set  $N_A = 2, 3, 4$  and compute the trace distance  $\Delta^{(2)}$  as a function of time in each case. The numerical results are shown in Fig. 6. We see the same qualitative behavior of the previous cases:  $\Delta^{(2)}$  decays with time to a finite-size plateau, which in turn decays exponentially in  $N$ , consistent with  $2^{-N/2}$ . As  $N_A$  increases, the size of the bath needs to increase proportionally—e.g., in the absence of conservation laws, it is known that  $N_B \geq kN_A$  is needed for equilibration of the  $k$ -th moment [8]; a similar constraint appears in Theorem 1. Thus for  $N_A > 2$  we see larger numerical values of the distance  $\Delta^{(2)}$ , but the trends as  $N \rightarrow \infty$  are unchanged.

Fig. 6 shows that the GSE is a surprisingly accurate description of the limiting ensemble already at the minimum nontrivial subsystem size of  $N_A = 2$ . This suggests



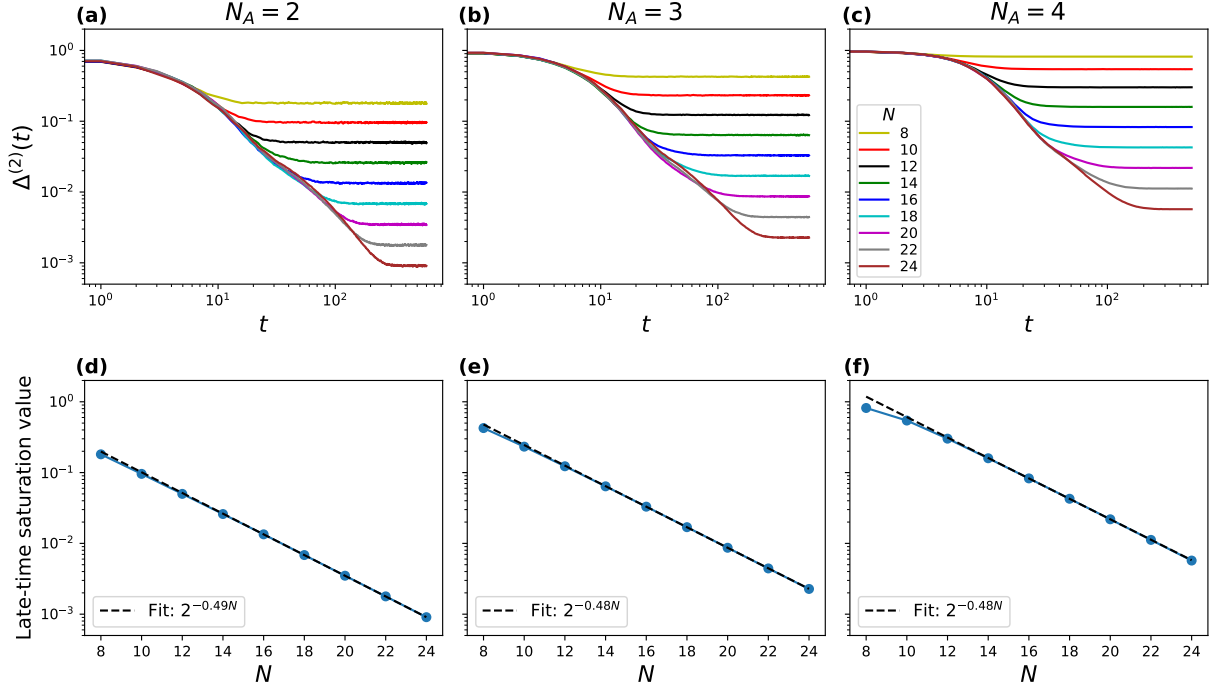


Figure 6. (a)-(c): Trace distance  $\Delta^{(2)}$  between the second moment of the projected ensemble and that of the GSE, Eq. (16), as a function of time, for the initial state in Eq. (30) with  $\theta = \pi/20$  and measurements in the  $z$  basis. The subsystem size  $N_A$  is held fixed at 2, 3, and 4 in (a), (b), (c), respectively, while the total system size  $N$  is varied. Results are averaged over 128 realizations of the random circuit. (d)-(f): Late-time average values of  $\Delta^{(2)}$ , extracted from (a)-(c), plotted against  $N$ . As  $N_A$  is increased, a proportionally larger value of  $N_B$  is required in order to converge to a universal ensemble, as expected. Nonetheless we see a decay of the late-time value of  $\Delta^{(2)}$  consistent with  $2^{-N/2}$  in all cases (dashed lines).

that the  $N_A \rightarrow \infty$  limit used in our replica limit calculation, App. B, is not in fact necessary for the validity of the result.

### B. Charge non-revealing measurements

Next we verify our predictions for  $x$ -basis measurements, which are charge-non-revealing. We again focus on the second moment ( $k = 2$ ) and consider the Néel state  $|01\rangle^{\otimes N/2}$  and  $X$ -basis product state  $|+\rangle^{\otimes N}$ . In the former case, the results of Sec. IV B suggest convergence to the Haar ensemble. The latter case falls outside the ones we could address analytically, but it is natural to conjecture the same outcome. For this reason we set the target ensemble to be the Haar ensemble and compute the distance  $\Delta^{(2)} = \frac{1}{2} \|\rho_{\mathcal{E}}^{(2)} - \rho_{\text{Haar}}^{(2)}\|_{\text{tr}}$ .

For the  $X$ -basis state, Fig. 7 (a), we can clearly see that  $\Delta^{(2)}$  decays to a late-time plateau that is exponentially small in the size of the total system  $N$ , consistent with deep thermalization to the Haar ensemble. For the Néel state, on the other hand, the convergence as a function of  $N$  appears considerably slower, as shown in Fig. 7 (b). The reason for these strong finite-size effects is due to the first moment:  $\rho_A$  (at late time, on average) is diagonal, with entries that depend only on the charge sector  $Q_A$

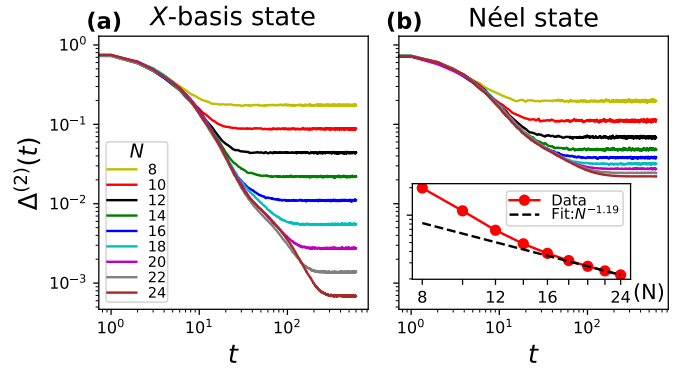


Figure 7. Trace distance  $\Delta^{(2)}$  between the second moment of the projected ensemble and the Haar ensemble, for the initial state in Eq. (30) with measurements in the  $x$  basis. (a)  $\theta = \pi/4$  ( $X$ -basis initial state).  $\Delta^{(2)}$  decays to a late-time plateau that is exponentially small in the size of the total system  $N$ . This result is identical to that of  $Z$ -basis measurement shown in Fig. 5. (b)  $\theta = 0$  (Néel initial state). The late-time plateau decays much more slowly in  $N$ . (Inset) A fit indicates a power-law decay consistent with  $\sim 1/N$  (the fit exponent  $N^{-1.19}$  is likely affected by strong finite-size effects due to a crossover from an exponential behavior at smaller  $N$ , to the asymptotic power-law behavior at large  $N$ ).

and are given by

$$\langle z | \rho_A | z \rangle = \binom{N_B}{Q_0 - Q_A} \binom{N}{Q_0}^{-1} \quad (34)$$

where  $z$  is any basis state of charge  $Q_A$  and  $Q_0 = N/2$ . These entries become  $Q_A$ -independent in the limit  $N_B \rightarrow \infty$ , so that  $\rho_A \rightarrow \mathbb{I}/2^{N_A}$  and it becomes possible to obtain deep thermalization to the Haar ensemble; but the convergence is only polynomial in  $1/N_B$ . Indeed we have

$$\begin{aligned} \binom{N_B}{Q_0 - Q_A} \binom{N}{Q_0}^{-1} &= \frac{N_B!}{N!} \frac{(N/2)!}{(N/2 - Q_A)!} \\ &\times \frac{(N/2)!}{(N/2 - N_A + Q_A)!} \end{aligned} \quad (35)$$

and, by making repeated use of the ‘birthday paradox’ asymptotics  $x!/(x-k)! = x^k \exp[-\binom{k}{2} \frac{1}{x} + O(1/x^2)]$  (valid for  $x \gg k$ ), we can conclude

$$\binom{N_B}{Q_0 - Q_A} \binom{N}{Q_0}^{-1} \simeq 2^{-N_A} e^{O(1/N)}, \quad (36)$$

where the coefficient of the  $1/N$  correction depends on  $Q_A$  and generically does not vanish. Therefore the trace distance between  $\rho_A$  and  $\rho_{\text{Haar}}^{(1)} = \mathbb{I}/2^{N_A}$  (first moment of the Haar ensemble) decays only as  $\sim 1/N$ . This error on the first moment also affects the second moment, and thus slows down the decay of  $\Delta^{(2)}$ . The inset to Fig. 7(b) indeed confirms a power-law decay in  $N$ , with an exponent close to  $-1$ .

In light of this, we repeat the calculation for a target ensemble that explicitly depends on  $N$ : we consider the Scrooge ensemble formed from the *finite- $N$*  average density matrix  $\rho_A(N)$ , with entries given in Eq. (34). Results for  $\Delta^{(2)}$  with this size-dependent target ensemble are shown in Fig. 8(a), and clearly display an exponential-in- $N$  convergence. Therefore we have exponential-in- $N$  convergence to the Scrooge ensemble  $\mathcal{E}_{\text{Scrooge}}[\rho_A(N)]$ , alongside  $\sim 1/N$  convergence of the latter toward the Haar ensemble.

Finally, we test the predictions of Sec. IV B on states of well-defined charge away from neutrality,  $Q_0 \neq N/2$ . The conjectured limiting ensemble in that case is the Scrooge ensemble for the appropriate density matrix  $\rho_A$ . We thus repeat our calculation for the initial state  $|0001\rangle^{\otimes N/4}$ , and again construct an  $N$ -dependent target ensemble based on the finite- $N$  reduced density matrix  $\rho_A(N)$ , Eq. (34) with  $Q_0 \mapsto N/4$ . Results, shown in Fig. 8(b), are again consistent with exponential-in- $N$  convergence. Specifically, we see a finite-size decay as  $2^{-H_2(\sigma)N/2}$ , with  $H_2(\sigma) = -\sigma \log_2(\sigma) - (1-\sigma) \log_2(1-\sigma)$  the binary entropy (in base 2) of the charge density  $\sigma = Q_0/N = 1/4$ . This is again consistent with the expectation of finite-size effects scaling as the inverse square root of Hilbert space dimension, since  $d_{Q_0} = \binom{N}{Q_0} \sim 2^{H_2(\sigma)N + o(N)}$ . These results support the conclusion of deep thermalization to the Scrooge ensemble under charge-non-revealing measurements on symmetric states.

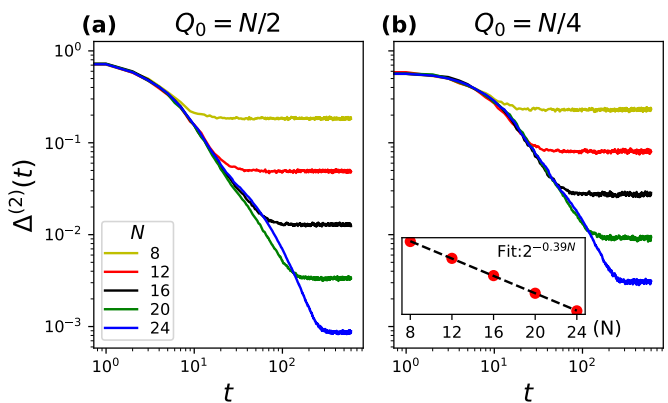


Figure 8. Trace distance  $\Delta^{(2)}$  between the second moment of the projected ensemble and the Scrooge ensemble formed from the finite- $N$  density matrix  $\rho_A$ . Measurements are performed in the  $x$  basis. (a) Néel initial state  $(|01\rangle^{\otimes N/2})$ , with total charge  $Q_0 = N/2$ . The late-time value of  $\Delta^{(2)}$  decays as  $\sim 2^{-N/2}$  (not shown). (b) Initial state  $|0001\rangle^{\otimes N/4}$ , with total charge  $Q_0 = N/4$ . Inset: The late-time value of  $\Delta^{(2)}$  decays exponentially in  $N$ ; a fit yields  $\sim 2^{-0.39N}$ , consistent with the expectation  $\sim 2^{-H_2(\sigma)N/2}$  where  $H_2(\sigma)$  is the binary entropy of the charge density  $\sigma$ , and  $H_2(1/4) \simeq 0.81$ .

### C. Higher moments

Here we have only reported data for the second moment,  $k = 2$ . To confirm that our predictions hold for higher moments as well, we report additional data in Appendix E on moments  $k = 3$  and 4. We focus on the case with the most complex target ensemble studied so far, that is, the case of states with intermediate charge fluctuations measured in the computational basis, Sec. V A 3. Our results are again consistent with deep thermalization to the GSE, providing strong evidence that all results observed in this Section would carry over to higher moments  $k > 2$ .

## VI. DISCUSSION

In this work, we have studied the phenomenon of deep thermalization, a novel form of quantum equilibration, in systems harboring a  $U(1)$  conserved charge. We have presented a general theory predicting a rich variety of limiting universal forms of the projected ensemble, influenced by charge fluctuations in the initial state and by the choice of measurement basis — which may or may not reveal information about the local charge density.

First, we have rigorously proven that maximally charge-revealing measurements on a random state of well-defined total charge yield a projected ensemble that breaks up into a direct sum of Haar ensembles on the individual charge sector of the subsystem of interest  $A$ . Then, by analytical calculations in a replica limit, we have shown that maximally charge-revealing measure-

ments on a state with arbitrary charge distribution  $p(Q)$  yield the “generalized Scrooge ensemble” (GSE). This is effectively a higher-moment generalization of the Gibbs state in standard quantum thermalization, though a crucial difference is that the latter depends only on the average charge of the system  $\langle Q \rangle = \sum_Q p(Q)Q$  via the chemical potential while the GSE depends on the full charge distribution  $p(Q)$ . By similar techniques, we have shown that charge-non-revealing measurements on a symmetric state yield a standard (i.e., not generalized) Scrooge ensemble, which reduces to the Haar ensemble if the state is charge-neutral. These results are summarized in Table I. Our analytical derivations recover the rigorous result of Theorem 1 in the relevant setting, and are further corroborated by exact numerical simulations of  $U(1)$ -symmetric random unitary circuits.

A notable aspect of our results is that they recover the same outcome in two settings that are microscopically very different: on the one hand, a state with equilibrium charge fluctuations subjected to maximally charge-revealing ( $z$ ) measurements, Sec. IV A 2; on the other, a state with no charge fluctuations subjected to charge-non-revealing ( $x$ ) measurements, Sec. IV B. Somewhat counterintuitively, both cases fall under the ‘non-revealing’ universality: even though in the former case the measurements fully reveal the charge  $Q_B$  of the bath, due to the equilibrium nature of the charge fluctuations, we gain no information about the charge  $Q_A$  of the subsystem of interest, so that the measurements are effectively non-revealing. Recovering the same outcome for both cases is further evidence that deep thermalization is a universal phenomenon dictated by principles of maximum entropy [14] and minimum accessible information [15, 45], and otherwise insensitive to microscopic details.

Our results on deep thermalization with a  $U(1)$  conserved charge are closely related to recent works on deep thermalization in energy-conserving (Hamiltonian) systems, where one also obtains a GSE for ‘energy-revealing’ measurements and a Scrooge ensemble (which reduces to the Haar ensemble at infinite temperature) for ‘energy-non-revealing’ measurements [8, 14]. A distinct conceptual feature of our setup relative to the Hamiltonian one is that the GSE is built out of a limited (linear in  $N$ ) amount of data, namely the distribution  $p(Q)$  and the possible charge measurement outcomes  $\{Q_B\}$  on the bath. The Hamiltonian case instead appears to depend

on an exponential amount of data (e.g. all possible bit-strings measured on the bath) [14].

It is possible that the latter structure would also arise in our  $U(1)$  charge-conserving setting under general, ‘partially charge-revealing’ measurement bases, which are neither ‘maximally charge-revealing’ ( $z$  basis) nor ‘charge-non-revealing’ ( $x$ - $y$  plane bases). We leave this interesting scenario, as well as a full study of the similarities and differences between the case of Abelian on-site symmetry and energy conservation, for future work. A possible intermediate step would be to consider the effect of *non-Abelian* symmetries, such as  $SU(2)$ , or non-on-site symmetries such as translation [44]. These generally do not admit a local, fully-revealing basis—i.e., they do not have a complete basis of disentangled eigenstates, which makes them more similar to the case of energy conservation. More broadly, non-Abelian symmetry has been shown to have remarkably strong effects on thermalization [52–54] and on the entanglement of post-measurement states [55, 56], and we expect its effect on deep thermalization to be no less rich.

From a practical stand-point, the formation of unitary designs, whether in individual charge sectors or across the whole Hilbert space, have potential applications in quantum information processing on systems (like certain ultra-cold atom-based quantum simulators) whose dynamics obey a particle number conservation law. Applications include classical shadow tomography and more generally randomized measurements for quantum state learning on analog simulators [34, 57, 58], randomized benchmarking [59] and process tomography [60], initialization of random states for quantum simulation based on typicality [61–64], etc. The case of Haar ensembles in individual charge sectors is especially interesting as it allows to target (with a polynomial postselection overhead) highly random states of fixed charge, enabling charge-resolved variants of all the aforementioned protocols.

## ACKNOWLEDGMENTS

Numerical simulations were performed in part on HPC resources provided by the Texas Advanced Computing Center (TACC) at the University of Texas at Austin. W. W. H. is supported by the Singapore NRF Fellowship, NRF-NRFF15-2023-0008, and the CQT Bridging Fund.

- 
- [1] M. Srednicki, Chaos and quantum thermalization, *Physical Review E* **50**, 888 (1994).
  - [2] M. Rigol, V. Dunjko, and M. Olshanii, Thermalization and its mechanism for generic isolated quantum systems, *Nature* **452**, 854 (2008).
  - [3] R. Nandkishore and D. A. Huse, Many-Body Localization and Thermalization in Quantum Statistical Mechanics, *Annual Review of Condensed Matter Physics* **6**, 15 (2015).
  - [4] L. D’Alessio, Y. Kafri, A. Polkovnikov, and M. Rigol, From quantum chaos and eigenstate thermalization to statistical mechanics and thermodynamics, *Advances in Physics* **65**, 239 (2016).
  - [5] A. M. Kaufman, M. E. Tai, A. Lukin, M. Rispoli, R. Schittko, P. M. Preiss, and M. Greiner, Quantum thermalization through entanglement in an isolated many-

- body system, *Science* **353**, 794 (2016).
- [6] D. A. Abanin, E. Altman, I. Bloch, and M. Serbyn, Colloquium: Many-body localization, thermalization, and entanglement, *Reviews of Modern Physics* **91**, 021001 (2019).
- [7] J. Choi, A. L. Shaw, I. S. Madjarov, X. Xie, R. Finkelstein, J. P. Covey, J. S. Cotler, D. K. Mark, H.-Y. Huang, A. Kale, H. Pichler, F. G. S. L. Brandao, S. Choi, and M. Endres, Preparing random states and benchmarking with many-body quantum chaos, *Nature* **613**, 468 (2023).
- [8] J. S. Cotler, D. K. Mark, H.-Y. Huang, F. Hernandez, J. Choi, A. L. Shaw, M. Endres, and S. Choi, Emergent Quantum State Designs from Individual Many-Body Wave Functions, *PRX Quantum* **4**, 010311 (2023).
- [9] W. W. Ho and S. Choi, Exact Emergent Quantum State Designs from Quantum Chaotic Dynamics, *Physical Review Letters* **128**, 060601 (2022).
- [10] M. Ippoliti and W. W. Ho, Dynamical Purification and the Emergence of Quantum State Designs from the Projected Ensemble, *PRX Quantum* **4**, 030322 (2023).
- [11] M. Ippoliti and W. W. Ho, Solvable model of deep thermalization with distinct design times, *Quantum* **6**, 886 (2022).
- [12] T. Bhore, J.-Y. Desaulles, and Z. Papic, Deep thermalization in constrained quantum systems, *Physical Review B* **108**, 104317 (2023).
- [13] M. Lucas, L. Piroli, J. De Nardis, and A. De Luca, Generalized deep thermalization for free fermions, *Physical Review A* **107**, 032215 (2023).
- [14] D. K. Mark, F. Surace, A. Elben, A. L. Shaw, J. Choi, G. Refael, M. Endres, and S. Choi, A Maximum Entropy Principle in Deep Thermalization and in Hilbert-Space Ergodicity, [arXiv:2403.11970v1](https://arxiv.org/abs/2403.11970v1) (2024).
- [15] C. Liu, Q. C. Huang, and W. W. Ho, Deep thermalization in continuous-variable quantum systems, [arXiv:2405.05470v1](https://arxiv.org/abs/2405.05470v1) (2024).
- [16] A. A. Mele, Introduction to Haar Measure Tools in Quantum Information: A Beginner's Tutorial, *Quantum* **8**, 1340 (2024).
- [17] J. M. Renes, R. Blume-Kohout, A. J. Scott, and C. M. Caves, Symmetric informationally complete quantum measurements, *Journal of Mathematical Physics* **45**, 2171 (2004).
- [18] A. Ambainis and J. Emerson, Quantum t-designs: t-wise Independence in the Quantum World, in *Twenty-Second Annual IEEE Conference on Computational Complexity (CCC'07)* (2007) pp. 129–140.
- [19] P. W. Claeys and A. Lamacraft, Emergent quantum state designs and biunitarity in dual-unitary circuit dynamics, *Quantum* **6**, 738 (2022).
- [20] H. Wilming and I. Roth, High-temperature thermalization implies the emergence of quantum state designs, [arXiv:2202.01669](https://arxiv.org/abs/2202.01669) [cond-mat, physics:math-ph, physics:quant-ph] (2022).
- [21] V. Khemani, A. Vishwanath, and D. A. Huse, Operator Spreading and the Emergence of Dissipative Hydrodynamics under Unitary Evolution with Conservation Laws, *Phys. Rev. X* **8**, 031057 (2018).
- [22] T. Rakovszky, F. Pollmann, and C. W. von Keyserlingk, Diffusive Hydrodynamics of Out-of-Time-Ordered Correlators with Charge Conservation, *Phys. Rev. X* **8**, 031058 (2018).
- [23] N. Hunter-Jones, Operator growth in random quantum circuits with symmetry, [arXiv:1812.08219](https://arxiv.org/abs/1812.08219) (2018).
- [24] U. Agrawal, A. Zabalo, K. Chen, J. H. Wilson, A. C. Potter, J. H. Pixley, S. Gopalakrishnan, and R. Vasseur, Entanglement and Charge-Sharpener Transitions in U(1) Symmetric Monitored Quantum Circuits, *Physical Review X* **12**, 041002 (2022).
- [25] A. Rath, V. Vitale, S. Murciano, M. Votto, J. Dubail, R. Kueng, C. Branciard, P. Calabrese, and B. Vermersch, Entanglement Barrier and its Symmetry Resolution: Theory and Experimental Observation, *PRX Quantum* **4**, 010318 (2023).
- [26] F. Ares, S. Murciano, and P. Calabrese, Entanglement asymmetry as a probe of symmetry breaking, *Nature Communications* **14**, 2036 (2023).
- [27] C. Jonay, J. F. Rodriguez-Nieva, and V. Khemani, Slow thermalization and subdiffusion in  $U(1)$  conserving Floquet random circuits, *Physical Review B* **109**, 024311 (2024).
- [28] C. M. Langlett and J. F. Rodriguez-Nieva, Entanglement patterns of quantum chaotic Hamiltonians with a scalar U(1) charge, [arXiv:2403.10600v1](https://arxiv.org/abs/2403.10600v1) (2024).
- [29] X. Turkeshi, P. Calabrese, and A. De Luca, Quantum Mpemba Effect in Random Circuits, [arXiv:2405.14514](https://arxiv.org/abs/2405.14514) (2024).
- [30] M. P. A. Fisher, V. Khemani, A. Nahum, and S. Vijay, Random Quantum Circuits, *Annual Review of Condensed Matter Physics* **14**, 335 (2023).
- [31] S. Liu, H.-K. Zhang, S. Yin, and S.-X. Zhang, Symmetry restoration and quantum mpemba effect in symmetric random circuits (2024), [arXiv:2403.08459](https://arxiv.org/abs/2403.08459) [quant-ph].
- [32] Z. Li, H. Zheng, J. Liu, L. Jiang, and Z.-W. Liu, Designs from local random quantum circuits with su(d) symmetry (2024), [arXiv:2309.08155](https://arxiv.org/abs/2309.08155) [quant-ph].
- [33] Z. Li, H. Zheng, Y. Wang, L. Jiang, Z.-W. Liu, and J. Liu, Su(d)-symmetric random unitaries: Quantum scrambling, error correction, and machine learning (2023), [arXiv:2309.16556](https://arxiv.org/abs/2309.16556) [quant-ph].
- [34] S. N. Hearth, M. O. Flynn, A. Chandran, and C. R. Laumann, Efficient Local Classical Shadow Tomography with Number Conservation, *Physical Review Letters* **133**, 060802 (2024).
- [35] H. Zheng, Z. Li, and Z.-W. Liu, Efficient quantum pseudorandomness in the presence of conservation laws, to appear (2024), .
- [36] S. J. Garratt and E. Altman, Probing Postmeasurement Entanglement without Postselection, *PRX Quantum* **5**, 030311 (2024).
- [37] M. McGinley, Postselection-Free Learning of Measurement-Induced Quantum Dynamics, *PRX Quantum* **5**, 020347 (2024).
- [38] J. C. Hoke, M. Ippoliti, E. Rosenberg, D. Abanin, R. Acharya, T. I. Andersen, M. Ansmann, F. Arute, K. Arya, A. Asfaw, J. Atalaya, J. C. Bardin, A. Bengtsson, G. Bortoli, A. Bourassa, J. Bovaird, *et al.*, Measurement-induced entanglement and teleportation on a noisy quantum processor, *Nature* **622**, 481 (2023).
- [39] D. A. Roberts and B. Yoshida, Chaos and complexity by design, *Journal of High Energy Physics* **2017**, 121 (2017).
- [40] E. Knill, D. Leibfried, R. Reichle, J. Britton, R. B. Blakestad, J. D. Jost, C. Langer, R. Ozeri, S. Seidelin, and D. J. Wineland, Randomized benchmarking of quantum gates, *Physical Review A* **77**, 012307 (2008).
- [41] C. Dankert, R. Cleve, J. Emerson, and E. Livine, Exact and approximate unitary 2-designs and their applica-



- tion to fidelity estimation, *Physical Review A* **80**, 012304 (2009).
- [42] H.-Y. Huang, R. Kueng, and J. Preskill, Predicting many properties of a quantum system from very few measurements, *Nature Physics* **16**, 1050 (2020).
- [43] C. Lancien and C. Majenz, Weak approximate unitary designs and applications to quantum encryption, *Quantum* **4**, 313 (2020).
- [44] N. D. Varikuti and S. Bandyopadhyay, Unraveling the emergence of quantum state designs in systems with symmetry, arXiv:2402.08949 [10.48550/arXiv.2402.08949](https://arxiv.org/abs/10.48550/arXiv.2402.08949) (2024).
- [45] R. Jozsa, D. Robb, and W. K. Wootters, Lower bound for accessible information in quantum mechanics, *Physical Review A* **49**, 668 (1994).
- [46] S. Goldstein, J. L. Lebowitz, R. Tumulka, and N. Zanghi, On the Distribution of the Wave Function for Systems in Thermal Equilibrium, *Journal of Statistical Physics* **125**, 1193 (2006).
- [47] S. Goldstein, J. L. Lebowitz, C. Mastrodonato, R. Tumulka, and N. Zanghi, Universal Probability Distribution for the Wave Function of a Quantum System Entangled with its Environment, *Communications in Mathematical Physics* **342**, 965 (2016).
- [48] M. Ledoux, The Concentration of Measure Phenomenon, *Mathematical Surveys and Monographs* **89**, <https://doi.org/10.1090/surv/089> (2001).
- [49] S. Pilatowsky-Cameo, C. B. Dag, W. W. Ho, and S. Choi, Complete Hilbert-Space Ergodicity in Quantum Dynamics of Generalized Fibonacci Drives, *Physical Review Letters* **131**, 250401 (2023).
- [50] S. Pilatowsky-Cameo, I. Marvian, S. Choi, and W. W. Ho, Hilbert-Space Ergodicity in Driven Quantum Systems: Obstructions and Designs, arXiv:2402.06720 [10.48550/arXiv.2402.06720](https://arxiv.org/abs/10.48550/arXiv.2402.06720) (2024).
- [51] I. Marvian, Theory of Quantum Circuits with Abelian Symmetries, arXiv:2302.12466v2 (2023).
- [52] C. Murthy, A. Babakhani, F. Iniguez, M. Srednicki, and N. Yunger Halpern, Non-Abelian Eigenstate Thermalization Hypothesis, *Physical Review Letters* **130**, 140402 (2023).
- [53] S. Majidy, A. Lasek, D. A. Huse, and N. Yunger Halpern, Non-Abelian symmetry can increase entanglement entropy, *Physical Review B* **107**, 045102 (2023).
- [54] S. Majidy, W. F. Braasch, A. Lasek, T. Upadhyaya, A. Kalev, and N. Yunger Halpern, Noncommuting conserved charges in quantum thermodynamics and beyond, *Nature Reviews Physics* **5**, 689 (2023).
- [55] S. Majidy, U. Agrawal, S. Gopalakrishnan, A. C. Potter, R. Vasseur, and N. Y. Halpern, Critical phase and spin sharpening in SU(2)-symmetric monitored quantum circuits, *Physical Review B* **108**, 054307 (2023).
- [56] X. Feng, N. Fishchenko, S. Gopalakrishnan, and M. Ippoliti, Charge and Spin Sharpening Transitions on Dynamical Quantum Trees, arXiv:2405.13894v1 (2024).
- [57] M. C. Tran, D. K. Mark, W. W. Ho, and S. Choi, Measuring Arbitrary Physical Properties in Analog Quantum Simulation, *Physical Review X* **13**, 011049 (2023).
- [58] M. McGinley and M. Fava, Shadow Tomography from Emergent State Designs in Analog Quantum Simulators, *Physical Review Letters* **131**, 160601 (2023).
- [59] C. H. Baldwin, B. J. Bjork, J. P. Gaebler, D. Hayes, and D. Stack, Subspace benchmarking high-fidelity entangling operations with trapped ions, *Physical Review Research* **2**, 013317 (2020).
- [60] I. Marvian, Restrictions on realizable unitary operations imposed by symmetry and locality, *Nature Physics* **18**, 283 (2022).
- [61] S. Goldstein, J. L. Lebowitz, R. Tumulka, and N. Zanghi, Canonical Typicality, *Physical Review Letters* **96**, 050403 (2006).
- [62] X. Mi, M. Ippoliti, C. Quintana, A. Greene, Z. Chen, J. Gross, F. Arute, K. Arya, J. Atalaya, R. Babush, J. C. Bardin, J. Basso, A. Bengtsson, A. Bilmes, A. Bourassa, L. Brill, *et al.*, Time-crystalline eigenstate order on a quantum processor, *Nature* **601**, 531 (2022).
- [63] J. Richter and A. Pal, Simulating Hydrodynamics on Noisy Intermediate-Scale Quantum Devices with Random Circuits, *Physical Review Letters* **126**, 230501 (2021).
- [64] T. I. Andersen, N. Astrakhantsev, A. H. Karamlou, J. Berndtsson, J. Motruk, A. Szasz, J. A. Gross, A. Schuckert, T. Westerhout, Y. Zhang, E. Forati, D. Rossi, B. Kobrin, A. Di Paolo, A. R. Klots, I. Drozdov, *et al.*, Thermalization and Criticality on an Analog-Digital Quantum Simulator, arXiv:2405.17385 [10.48550/arXiv.2405.17385](https://arxiv.org/abs/10.48550/arXiv.2405.17385) (2024).

### Appendix A: Proof of Theorem 1

Here we prove Theorem 1 stated in the main text, which is that with high probability, the projected ensemble  $\mathcal{E}_A$  of a Haar random  $U(1)$ -symmetric state, constructed using charge-revealing computational basis ( $z$ ) measurements, is the direct sum ensemble. We restate Theorem 1 in slightly more formal fashion:

**Theorem 1.** *Let  $|\Psi\rangle$  be a Haar random state on  $N$  qubits with definite charge  $Q_0$ , so that the state lives in a Hilbert space with dimension  $d_{Q_0} = \binom{N}{Q_0}$ . Construct the projected ensemble  $\mathcal{E}_A$  on  $N_A$  qubits, using measurements of  $B$  in the computational ( $z$ ) basis. Then as long as*

$$d_{Q_0} \geq \frac{18\pi^3(2k-1)^2(N_A+1)^2 d_A^{4k}}{\epsilon^2} (\log(2/\delta) + \log(2C_k d_A^{2k} N_A^{1-k})), \quad (\text{A1})$$

( $C_k$  is a numerical constant depending on  $k$  but not depending on  $N_A$ ) with probability at least  $1-\delta$  the trace difference between the  $k$ -th moments of the projected ensemble and the ‘direct sum (DS)’ ensemble, obeys

$$\frac{1}{2} \|\rho_{\mathcal{E}}^{(k)} - \rho_{DS, Q_0}^{(k)}\| \leq \epsilon, \quad (\text{A2})$$

where

$$\rho_{DS, Q_0}^{(k)} = \bigoplus \pi(Q_A|Q_0) \rho_{\text{Haar}, A, Q_A}^{(k)}. \quad (\text{A3})$$

Above,  $\rho_{\text{Haar}, A, Q_A}^{(k)}$  is the  $k$ -th moment of the Haar ensemble on states on  $A$  with fixed charge  $Q_A$ ,  $d_{Q_A} = \binom{N_A}{Q_A}$  is the dimension of charge sector  $Q_A$  on  $N_A$  qubits, and the probability  $\pi(Q_A|Q_0) = d_{Q_A} d_{Q_B} / d_{Q_0}$ , where  $d_{Q_B} = \binom{N-N_A}{Q_0-Q_A}$ .

Letting  $\sigma \equiv Q_0/N \in [0, 1]$ , the condition on  $d_{Q_0}$  can be satisfied with

$$N_B H(\sigma) = \Omega(kN_A + \log(\epsilon^{-1}) + \log \log(\delta^{-1})) \quad (\text{A4})$$

where  $H(\sigma) = -\sigma \log \sigma - (1-\sigma) \log(1-\sigma)$ .

*Proof.* We break the proof in two parts. We first show that the  $k^{\text{th}}$ -moment of the projected ensemble  $\mathcal{E}_A$  averaged over all Haar random  $U(1)$ -symmetric generator states  $|\Phi\rangle$  is exactly the  $k^{\text{th}}$ -moment of the direct sum ensemble, i.e.

$$\mathbb{E}_{\Phi \sim \text{Haar}(\mathcal{H}_{Q_0})} \left[ \sum_z \frac{(|\tilde{\psi}_z\rangle\langle\tilde{\psi}_z|)^{\otimes k}}{\langle\tilde{\psi}_z|\tilde{\psi}_z\rangle^{k-1}} \right] = \bigoplus_{Q_A} \pi(Q_A|Q_0) \rho_{\text{Haar}, A, Q_A}^{(k)} = \rho_{DS, Q_0}^{(k)}. \quad (\text{A5})$$

To do so we break the summation  $\sum_z [\dots] = \sum_{Q_B} \sum_{z_{Q_B}} [\dots]$  into sums over charge sectors  $Q_B$  and outcome strings  $z_{Q_B}$  of fixed charge  $Q_B$  and define the normalized state  $|\psi_{z_{Q_B}}\rangle = |\tilde{\psi}_{z_{Q_B}}\rangle / \sqrt{p(z_{Q_B})}$  with  $p(z_{Q_B}) = \langle\tilde{\psi}_{z_{Q_B}}|\tilde{\psi}_{z_{Q_B}}\rangle$ . This allows us to write the LHS as

$$\sum_{Q_B} \sum_{z_{Q_B}} \mathbb{E}_{\Phi \sim \text{Haar}(\mathcal{H}_{Q_0})} \left[ \left( |\psi_{z_{Q_B}}\rangle\langle\psi_{z_{Q_B}}| \right)^{\otimes k} p(z_{Q_B}) \right]. \quad (\text{A6})$$

Then we note that we can write  $|\Phi\rangle = U|Q_0\rangle$  where  $U$  is a charge-conserving unitary and  $|Q_0\rangle$  is any fixed, reference state with charge  $Q_0$ , and the Haar averaging of the states comes from Haar averaging the unitaries  $U$ . Because of the left invariance of the Haar measure, we can send  $U \rightarrow (U_A \otimes \mathbb{I}_B)U$  where  $U_A$  is *any* charge-conserving unitary on  $A$ , and all expected values remain invariant. But under this transformation  $p(z_{Q_B})$  is invariant while  $|\psi_{z_{Q_B}}\rangle\langle\psi_{z_{Q_B}}| \rightarrow U_A |\psi_{z_{Q_B}}\rangle\langle\psi_{z_{Q_B}}| U_A^\dagger$ , so the LHS equals

$$\sum_{Q_B} \sum_{z_{Q_B}} \mathbb{E}_{\Phi \sim \text{Haar}(\mathcal{H}_{Q_0})} \left[ \left( U_A |\psi_{z_{Q_B}}\rangle\langle\psi_{z_{Q_B}}| U_A^\dagger \right)^{\otimes k} p(z_{Q_B}) \right]. \quad (\text{A7})$$

We are also free to average over  $U_A$  in any fashion without changing the expected value; a convenient averaging is to also *Haar average* over  $U_A$ . Then we get

$$\begin{aligned}
& \sum_{Q_B} \sum_{z_{Q_B}} \mathbb{E}_{\Phi \sim \text{Haar}(\mathcal{H}_{Q_0})} \left[ \left( U_A |\psi_{z_{Q_B}}\rangle \langle \psi_{z_{Q_B}}| U_A^\dagger \right)^{\otimes k} p(z_{Q_B}) \right] \\
&= \sum_{Q_B} \sum_{z_{Q_B}} \mathbb{E}_{\Phi \sim \text{Haar}(\mathcal{H}_{Q_0})} \left[ \mathbb{E}_{U_A \sim \text{Haar}(\mathcal{H}_{Q_A})} \left[ \left( U_A |\psi_{z_{Q_B}}\rangle \langle \psi_{z_{Q_B}}| U_A^\dagger \right)^{\otimes k} \right] p(z_{Q_B}) \right] \\
&= \sum_{Q_B} \sum_{z_{Q_B}} \mathbb{E}_{\Phi \sim \text{Haar}(\mathcal{H}_{Q_0})} \left[ \rho_{\text{Haar}, A, Q_A}^{(k)} p(z_{Q_B}) \right] \\
&= \sum_{Q_B} \rho_{\text{Haar}, A, Q_A}^{(k)} \sum_{z_{Q_B}} \mathbb{E}_{\Phi \sim \text{Haar}(\mathcal{H}_{Q_0})} [p(z_{Q_B})] \\
&= \sum_{Q_B} \rho_{\text{Haar}, A, Q_A}^{(k)} \left( \frac{d_{Q_A} d_{Q_B}}{d_{Q_0}} \right) \\
&= \bigoplus_{Q_A} \pi(Q_A | Q_0) \rho_{\text{Haar}, A, Q_A}^{(k)}. \tag{A8}
\end{aligned}$$

Above, we used that the Haar average over  $U_A$  of  $k$  copies of a pure state with definite charge  $Q_A$  yields  $\rho_{\text{Haar}, A, Q_A}^{(k)}$ , and also that the sum over  $Q_B$  is equivalent to the sum over  $Q_A$ .

Having shown the assertion [A5](#), we proceed with the second part by bounding the deviation of  $k^{\text{th}}$  moment of the ensemble  $\mathcal{E}_A$  obtained from a single instance of a Haar random symmetric  $|\Phi\rangle$ , from the average behavior. To that end, we will use a standard concentration of measure lemma, which is [\[48\]](#)

**Lemma 1 (Levy)** *Let  $f : \mathbb{S}^{2d-1} \rightarrow \mathbb{R}$  be Lipschitz continuous i.e. satisfying  $|f(v) - f(w)| \leq \eta \|v - w\|_2$  for some Lipschitz constant  $\eta < \infty$ . Then, for any  $\delta \geq 0$ , we have*

$$\text{Prob}_{\Phi \sim \text{Haar}(\mathcal{H})} [|f(\Phi) - \mathbb{E}_{\Psi \sim \text{Haar}(\mathcal{H})} [f(\Psi)]| \geq \delta] \leq 2 \exp \left( -\frac{2d\delta^2}{9\pi^3\eta^2} \right). \tag{A9}$$

Define the function  $f$ ,

$$f(|\Phi\rangle) = \sum_z \frac{(|\tilde{\psi}_z\rangle \langle \tilde{\psi}_z|)^{\otimes k}}{\langle \tilde{\psi}_z | \tilde{\psi}_z \rangle^{k-1}}. \tag{A10}$$

We can break the sum over outcomes  $z$  again as

$$f(|\Phi\rangle) = \sum_{Q_B} \sum_{z_{Q_B}} \frac{(|\tilde{\psi}_{z_{Q_B}}\rangle \langle \tilde{\psi}_{z_{Q_B}}|)^{\otimes k}}{\langle \tilde{\psi}_{z_{Q_B}} | \tilde{\psi}_{z_{Q_B}} \rangle^{k-1}} =: \sum_{Q_B} f_{Q_B}(|\Phi\rangle). \tag{A11}$$

Thus consider the function  $f_{Q_B, ij}(|\Phi\rangle) : \mathbb{S}^{2d_{Q_0}-1} \rightarrow \mathbb{R}$  as

$$f_{Q_B, ij}(|\Phi\rangle) = \langle i | \left( \sum_{z_{Q_B}} \frac{(|\tilde{\psi}_{z_{Q_B}}\rangle \langle \tilde{\psi}_{z_{Q_B}}|)^{\otimes k}}{\langle \tilde{\psi}_{z_{Q_B}} | \tilde{\psi}_{z_{Q_B}} \rangle^{k-1}} \right) | j \rangle \tag{A12}$$

where  $|i\rangle = \otimes_{l=1}^k |i^{(l)}\rangle$  and  $|i^{(l)}\rangle$  is a basis element of  $\mathcal{H}^{Q_A}$ . From Lemma 2 of Ref. [\[8\]](#), we have that a Lipschitz constant for  $f_{Q_B, ij}$  is  $\eta = 2(2k-1)$ .

Now we apply Levy's lemma to  $f_{Q_B, ij}$  which gives

$$\text{Prob}_{\Phi \sim \text{Haar}(\mathcal{H}_{Q_0})} [|f_{Q_B, ij}(\Phi) - \mathbb{E}_{\Psi \sim \text{Haar}(\mathcal{H}_{Q_0})} [f_{Q_B, ij}(\Psi)]| \geq \epsilon] \leq 2 \exp \left( -\frac{2d_{Q_0}\epsilon^2}{9\pi^3 4(2k-1)^2} \right). \tag{A13}$$

A union bound on entries  $(i, j)$  and re-scaling  $\epsilon \rightarrow \epsilon/d_{Q_A}^{2k}$  gives

$$\begin{aligned}
& \text{Prob}_{\Phi \sim \text{Haar}(\mathcal{H}_{Q_0})} \left[ \left| f_{Q_B, ij}(\Phi) - \mathbb{E}_{\Psi \sim \text{Haar}(\mathcal{H}_{Q_0})} [f_{Q_B, ij}(\Psi)] \right| \geq \frac{\epsilon}{d_{Q_A}^{2k}}, \text{ for some } i, j \right] \\
& \leq 2d_{Q_A}^{2k} \exp \left( -\frac{d_{Q_0}\epsilon^2}{18\pi^3(2k-1)^2 d_{Q_A}^{4k}} \right). \tag{A14}
\end{aligned}$$

Define the entrywise (e) norm as  $\|A\|_{e,1} \equiv \sum_{i,j} |A_{ij}|$  and note that,

$$\begin{aligned} \text{Prob}[|A_{ij}| \geq \epsilon/N, \text{ for some } (i,j)] &= 1 - \text{Prob}[|A_{ij}| < \epsilon/N, \text{ for all } (i,j)] \\ &\geq 1 - \text{Prob}[\|A\|_{e,1} < \epsilon] \\ &= \text{Prob}[\|A\|_{e,1} \geq \epsilon], \end{aligned} \quad (\text{A15})$$

which gives

$$\text{Prob}_{\Phi \sim \text{Haar}(\mathcal{H}_{Q_0})} \left[ \left\| f_{Q_B}(\Phi) - \mathbb{E}_{\Psi \sim \text{Haar}(\mathcal{H}_{Q_0})} [f_{Q_B}(\Psi)] \right\|_{e,1} \geq \epsilon \right] \leq 2d_{Q_A}^{2k} \exp \left( -\frac{d_{Q_0} \epsilon^2}{18\pi^3 (2k-1)^2 d_{Q_A}^{4k}} \right) \quad (\text{A16})$$

Since  $\|A\|_{e,1} \geq \|A\|_1$ , we have

$$\text{Prob}[\|A\|_1 \geq \epsilon] \leq \text{Prob}[\|A\|_{e,1} \geq \epsilon] \quad (\text{A17})$$

using which we get (substituting the functional form of  $f_{Q_B}$ )

$$\text{Prob}_{\Phi \sim \text{Haar}(\mathcal{H}_{Q_0})} \left[ \left\| \sum_{z_{Q_B}} \frac{(|\tilde{\psi}_{z_{Q_B}}\rangle \langle \tilde{\psi}_{z_{Q_B}}|)^{\otimes k}}{\langle \tilde{\psi}_{z_{Q_B}} | \tilde{\psi}_{z_{Q_B}} \rangle^{k-1}} - \pi(Q_A|Q_0) \rho_{\text{Haar},A,Q_A}^{(k)} \right\|_1 \geq \epsilon \right] \leq 2d_{Q_A}^{2k} \exp \left( -\frac{d_{Q_0} \epsilon^2}{18\pi^3 (2k-1)^2 d_{Q_A}^{4k}} \right). \quad (\text{A18})$$

Next, we again apply a union bound for the different charge sectors and re-scale  $\epsilon \rightarrow \epsilon/(N_A + 1)$ . Then

$$\begin{aligned} \text{Prob}_{\Phi \sim \text{Haar}(\mathcal{H}_{Q_0})} \left[ \left\| \sum_{z_{Q_B}} \frac{(|\tilde{\psi}_{z_{Q_B}}\rangle \langle \tilde{\psi}_{z_{Q_B}}|)^{\otimes k}}{\langle \tilde{\psi}_{z_{Q_B}} | \tilde{\psi}_{z_{Q_B}} \rangle^{k-1}} - \pi(Q_A|Q_0) \rho_{\text{Haar},A,Q_A}^{(k)} \right\|_1 \geq \frac{\epsilon}{(N_A + 1)}, \text{ for some charge sector } Q_A \right] \\ \leq \sum_{Q_A} 2d_{Q_A}^{2k} \exp \left( -\frac{d_{Q_0} \epsilon^2}{18\pi^3 (N_A + 1)^2 (2k-1)^2 d_{Q_A}^{4k}} \right). \end{aligned} \quad (\text{A19})$$

For combining probabilities from different charge sectors we note that,

$$\begin{aligned} \text{Prob} \left[ \Delta_{Q_A}^{(k)} \geq \frac{\epsilon}{(N_A + 1)}, \text{ for some sector } Q_A \right] &= 1 - \text{Prob} \left[ \Delta_{Q_A}^{(k)} < \frac{\epsilon}{(N_A + 1)}, \text{ for all sectors } Q_A \right] \\ &\geq 1 - \text{Prob} \left[ \Delta^{(k)} < \epsilon \right] \\ &= \text{Prob} \left[ \Delta^{(k)} \geq \epsilon \right]. \end{aligned} \quad (\text{A20})$$

Thus we finally get

$$\begin{aligned} \text{Prob}_{\Phi \sim \text{Haar}(\mathcal{H}_{Q_0})} \left[ \left\| \sum_{Q_B} \sum_{z_{Q_B}} \frac{(|\tilde{\psi}_{z_{Q_B}}\rangle \langle \tilde{\psi}_{z_{Q_B}}|)^{\otimes k}}{\langle \tilde{\psi}_{z_{Q_B}} | \tilde{\psi}_{z_{Q_B}} \rangle^{k-1}} - \bigoplus_{Q_A} \pi(Q_A|Q_0) \rho_{\text{Haar},A,Q_A}^{(k)} \right\|_1 \geq \epsilon \right] \\ \leq \sum_{Q_A} 2d_{Q_A}^{2k} \exp \left( -\frac{d_{Q_0} \epsilon^2}{18\pi^3 (N_A + 1)^2 (2k-1)^2 d_{Q_A}^{4k}} \right). \end{aligned} \quad (\text{A21})$$

We can simplify the above expression, noting that  $d_{Q_A} \leq d_A = 2^{N_A}$ . Also,  $d_{Q_A} = \binom{N_A}{Q_A}$  and so  $\sum_{Q_A} d_{Q_A}^{2k} \leq C_k \sum_{Q_A} 2^{2N_A k} / N_A^k \leq C_k 2^{2N_A k} / N_A^{k-1}$  using known bounds on the central binomial coefficient which dominates all other binomial coefficients.  $C_k$  is a constant depending on  $k$  but not  $N_A$ .

So we get

$$\begin{aligned} \text{Prob}_{\Phi \sim \text{Haar}(\mathcal{H}_{Q_0})} \left[ \left\| \sum_z \frac{(|\tilde{\psi}_z\rangle \langle \tilde{\psi}_z|)^{\otimes k}}{\langle \tilde{\psi}_z | \tilde{\psi}_z \rangle^{k-1}} - \bigoplus_{Q_A} \pi(Q_A|Q_0) \rho_{\text{Haar},A,Q_A}^{(k)} \right\|_1 \geq \epsilon \right] \\ \leq 2C_k \frac{2^{2kN_A}}{N_A^{k-1}} \exp \left( -\frac{d_{Q_0} \epsilon^2}{18\pi^3 (N_A + 1)^2 (2k-1)^2 d_A^{4k}} \right). \end{aligned} \quad (\text{A22})$$



Thus, if

$$d_{Q_0} \geq \frac{18\pi^3(N_A + 1)^2(2k - 1)^2 d_A^{4k}}{\epsilon^2} \left( \log \left( \frac{2}{\delta} \right) + \log (2C_k d_A^{2k} N_A^{1-k}) \right) \quad (\text{A23})$$

then the  $k^{\text{th}}$  moment of the projected ensemble  $\mathcal{E}_A$  is  $\epsilon$ -close to  $\bigoplus_{Q_A} p(Q_A) \rho_{\text{Haar}, A, Q_A}^{(k)}$  with probability at least  $1 - \delta$ , as claimed.

Lastly, using Stirling's approximation

$$\begin{aligned} \log d_{Q_0} &= \log \left[ \binom{N}{Q} \right] \\ &\approx N \log N - N - ((\sigma N) \log(\sigma N) - (\sigma N) + (N - \sigma N) \log(N - \sigma N) - (N - \sigma N)) \\ &= N(-\sigma \log(\sigma) - (1 - \sigma) \log(1 - \sigma)) \\ &= NH(\sigma). \end{aligned} \quad (\text{A24})$$

The requirement on  $d_{Q_0}$  can be seen to be satisfied if the number of bath qubits obeys

$$N_B H(\sigma) = \Omega(kN_A + \log(\epsilon^{-1}) + \log \log(\delta^{-1})). \quad (\text{A25})$$

■

## Appendix B: Limiting form of the projected ensemble at late time

In this appendix we discuss the limiting form of the projected ensemble at late times in chaotic  $U(1)$ -symmetric dynamics for general initial states and measurement bases. First we derive a general, implicit form of the moment operator  $\rho^{(k)}$  averaged over random  $U(1)$ -symmetric transformations of the generator state; then we make progress, within a ‘replica limit’ approach, for two special cases of interest, namely (i) when the measurement basis is ‘maximally charge-revealing’ ( $z$  basis), and (ii) when the generator state is symmetric and the measurement basis is ‘charge non-revealing’ ( $x$  basis). From the expressions of the averaged moment operators  $\rho^{(k)}$  we are then able to reverse-engineer the form of the projected ensemble itself—though only in the limit of  $N, N_A \gg 1$ . Numerical evidence presented in Sec. V shows that, in practice, our results are correct in the thermodynamic limit  $N \rightarrow \infty$  even for small  $N_A$ .

### 1. Setup

We consider a general many-body pure state  $|\Psi\rangle = \sum_{Q=0}^N \sqrt{p(Q)} |\Phi_Q\rangle$ , with  $p(Q)$  the distribution of charge. We perform projective measurements on the bath in an as-of-yet unspecified basis  $\{|b\rangle_B\}_{b=1}^{d_B}$  of orthonormal pure states (we will later take these to be the  $X$  or  $Z$  basis). The  $k$ -th moment of the projected ensemble then reads

$$\rho_{\mathcal{E}(\Psi)}^{(k)} = \sum_{b=1}^{N_B} p(b) (|\psi_b\rangle\langle\psi_b|)^{\otimes k}, \quad p(b) = \langle\Psi| (\mathbb{I}_A \otimes |b\rangle\langle b|_B) |\Psi\rangle, \quad |\psi_b\rangle_A = {}_B\langle b|\Psi\rangle_{AB} / \sqrt{p(b)}. \quad (\text{B1})$$

Our ansatz is that general dynamics starting from a state with charge distribution  $p(Q)$  should converge to a projected ensemble whose moments are given by

$$\rho_{\text{target}}^{(k)} \equiv \mathbb{E}_{\{\Phi_Q \sim \text{Haar}(\mathcal{H}_Q)\}} \left[ \rho_{\mathcal{E}(\Psi)}^{(k)} \right]. \quad (\text{B2})$$

This is the average moment operator across all states  $|\Psi\rangle$  with the given charge distribution, where the state in each charge sector is taken to be Haar-random; the content of our conjecture is that this should be the moment operator not just on average, but for *almost all individual instances* of  $|\Psi\rangle$  with the given charge distribution, in a suitable thermodynamic limit.

## 2. General structure of the moment operators

Here we turn Eq. (B2) into a universal form that explicitly depends only on the charge distribution  $p(Q)$  and on the measurement basis  $\{|b\rangle\}$ .

Given input state  $|\Phi\rangle$ , we may in general define a joint distribution over measurement outcomes  $b$  and values of the charge on subsystem  $A$ ,  $Q_A$ , by

$$p(Q_A, b) = \langle \Psi | (\hat{\Pi}_{Q_A} \otimes |b\rangle\langle b|) | \Psi \rangle = p(b) \langle \psi_b | \hat{\Pi}_{Q_A} | \psi_b \rangle. \quad (\text{B3})$$

This immediately implies the following decomposition for the projected states,

$$|\psi_b\rangle = \sum_{Q_A} \sqrt{p(Q_A|b)} |\phi_{b, Q_A}\rangle, \quad (\text{B4})$$

where the states  $|\phi_{b, Q_A}\rangle$  belong to charge sector  $Q_A$  of subsystem  $A$ , and  $p(Q_A|b) = p(Q_A, b)/p(b)$  is the conditional distribution of charge  $Q_A$  given outcome  $b$  on the bath, derived from the joint distribution in Eq. (B3).

Plugging this expansion of the projected states  $|\psi_b\rangle$  into the expression for the moment operator yields

$$\begin{aligned} \rho_{\mathcal{E}}^{(k)} &= \sum_b p(b) \left( \sum_{Q_A} \sqrt{p(Q_A|b)} |\phi_{b, Q_A}\rangle \right)^{\otimes k} \left( \sum_{Q_A} \sqrt{p(Q_A|b)} \langle \phi_{b, Q_A}| \right)^{\otimes k} \\ &= \sum_b p(b) \sum_{\mathbf{Q}_A, \mathbf{Q}'_A} \prod_{i=1}^k \sqrt{p(Q_{A,i}|b)p(Q'_{A,i}|b)} \bigotimes_{i=1}^k |\phi_{b, Q_{A,i}}\rangle \langle \phi_{b, Q'_{A,i}}|, \end{aligned} \quad (\text{B5})$$

where  $\mathbf{Q}_A, \mathbf{Q}'_A \in \{0, \dots, N_A\}^k$  are strings of values of the charge in each Hilbert space replica.

Our ansatz Eq. (B2) is that the target ensemble should be invariant under  $U(1)$ -symmetric unitary transformations. A special case of such transformations is one that acts nontrivially only on  $A$ :  $U = V_A \otimes \mathbb{I}_B$ , where  $V$  conserves the value of  $Q_A$ . Given unitary invariance of the Haar measure, we can write

$$\mathbb{E}_{U \sim U(1)\text{-Haar}(\mathcal{H}_{AB})} (\dots) = \mathbb{E}_{U \sim U(1)\text{-Haar}(\mathcal{H}_{AB})} \left[ \mathbb{E}_{V \sim U(1)\text{-Haar}(\mathcal{H}_A)} (\dots) \right], \quad (\text{B6})$$

with ‘ $U(1)$ -Haar’ denoting the Haar measure over unitary matrices that preserve the  $U(1)$ -symmetry (this is a compact Lie group and so has a Haar measure). Then we can carry out the average over  $V$  (a random  $U(1)$ -symmetric unitary on  $A$  only) first. This has the effect of replacing the vectors  $|\phi_{b, Q_A}\rangle$  by Haar-random vectors in their respective sector, which we denote by  $|\phi_{Q_A}\rangle$ :

$$\rho_{\text{target}}^{(k)} = \sum_b \sum_{\mathbf{Q}_A, \mathbf{Q}'_A} \mathbb{E}_{\{\Phi_Q \sim \text{Haar}(\mathcal{H}_Q)\}} \left[ p(b) \prod_{i=1}^k \sqrt{p(Q_{A,i}|b)p(Q'_{A,i}|b)} \right]_{\{\phi_{Q_A} \sim \text{Haar}(\mathcal{H}_{Q_A})\}} \left[ \bigotimes_{i=1}^k |\phi_{Q_{A,i}}\rangle \langle \phi_{Q'_{A,i}}| \right] \quad (\text{B7})$$

The average thus breaks up into a numerical factor and an operator factor; this is analogous to the observation used in proving Theorem 1 on the statistical independence between  $p(z)$  and  $|\psi_z\rangle$ .

In carrying out the Haar average over states  $\{|\phi_{Q_A}\rangle\}$ , we note that the average vanishes due to random dephasing unless the charge strings  $\mathbf{Q}_A, \mathbf{Q}'_A$  have the same content. We can capture this constraint by introducing the notion of a ‘‘type’’:

$$\text{type}(\mathbf{Q}) = \vec{T} = (T_0, T_1, \dots, T_N) : \quad T_q = |\{i : Q_i = q\}|. \quad (\text{B8})$$

In words, the type of  $\mathbf{Q}$  is the list of multiplicities of elements in  $\mathbf{Q}$  ( $T_q$  is the number of times that the value  $q$  appears in the sequence  $\mathbf{Q}$ ). We denote the set of possible types for lists  $\mathbf{Q}$  of length  $k$ , where each entry is valued in  $\{0, \dots, N\}$ , as  $\mathcal{T}(k, N)$ . Then, to avoid a cancellation in Eq. (B7), we must have  $\text{type}(\mathbf{Q}) = \text{type}(\mathbf{Q}')$ . The sum over  $\mathbf{Q}, \mathbf{Q}'$  can thus be replaced by a sum over ‘‘types’’  $\vec{T} \in \mathcal{T}(k, N)$  and a separate sum over permutations  $\sigma, \tau \in S_k$ . The idea is that an ordered list  $\mathbf{Q}$  is fully specified by two things: its unsorted content (the type  $\vec{T}$ ) and its ordering (a permutation  $\sigma \in S_k$  of its elements). This decomposition, however, has some redundancy—specifically whenever  $\mathbf{Q}$  is degenerate, i.e. when  $T_q > 1$  for some  $q$ . In general, by summing over  $\sigma \in S_k$  we count the same state a number of times  $\prod_q (T_q!)$ .

With this in mind, we can rewrite Eq. (B7) as

$$\begin{aligned} \rho_{\text{target}}^{(k)} &= \sum_b \sum_{\vec{T} \in \mathcal{T}(k, N)} \mathbb{E}_{\{\Phi_Q \sim \text{Haar}(\mathcal{H}_Q)\}} \left[ p(b) \prod_{Q_A=0}^{N_A} p(Q_A|b)^{T_{Q_A}} \right] \prod_{Q_A=0}^{N_A} \frac{1}{(T_{Q_A}!)^2} \sum_{\sigma, \tau \in S_k} \hat{\sigma} \left( \bigotimes_{Q_A=0}^{N_A} \rho_{\text{Haar}, A, Q_A}^{(T_{Q_A})} \right) \hat{\tau} \\ &= \sum_b \sum_{\vec{T} \in \mathcal{T}(k, N)} \mathbb{E}_{\{\Phi_Q \sim \text{Haar}(\mathcal{H}_Q)\}} \left[ p(b) \prod_{Q_A=0}^{N_A} p(Q_A|b)^{T_{Q_A}} \right] \binom{k}{\vec{T}}^2 \hat{\Pi}_{\text{sym}}^{(k)} \left( \bigotimes_{Q_A=0}^{N_A} \rho_{\text{Haar}, A, Q_A}^{(T_{Q_A})} \right) \hat{\Pi}_{\text{sym}}^{(k)}. \end{aligned} \quad (\text{B9})$$

Here,  $\hat{\sigma}$  is the replica permutation operator associated to permutation  $\sigma \in S_k$ ,  $\rho_{\text{Haar}, A, Q_A}^{(m)}$  is the  $m$ -th moment operator of the Haar ensemble on charge sector  $Q_A$  in subsystem  $A$ , and in the second line we have introduced the projector on the symmetric subspace and the multinomial coefficient,

$$\hat{\Pi}_{\text{sym}} = \frac{1}{k!} \sum_{\sigma \in S_k} \hat{\sigma}, \quad \binom{k}{\vec{T}} = \frac{k!}{T_0! \cdots T_N!} \quad (\text{B10})$$

(note that  $\sum_{Q_A=0}^{N_A} T_{Q_A} = k$ , so  $\vec{T}$  is a partition of  $k$ ).

It remains to calculate the numerical coefficients

$$f_p(\vec{T}, b) = \mathbb{E}_{\{\Phi_Q \sim \text{Haar}(\mathcal{H}_Q)\}} \left[ p(b) \prod_{Q_A} p(Q_A|b)^{T_{Q_A}} \right]. \quad (\text{B11})$$

This calculation is not straightforward due to the nontrivial dependence on the initial charge-sector states  $\{\Phi_Q\}$  to be averaged over. However, it can be carried out in an approximate way in several cases of interest, as we will show next.

### 3. Charge-revealing measurements on general states

Here we focus on the case of  $Z$ -basis measurements ( $b \mapsto z$ ) on arbitrary initial states, i.e., we place no restrictions on  $p(Q)$ . We will compute the  $f_p(\vec{T}, z)$  coefficients from Eq. (B11) within a replica limit approach, then perform an approximation of large Hilbert space dimension to express the resulting moment operator in a simpler way, and deduce a form of the projected ensemble compatible with such moment operators. The result is the generalized Scrooge ensemble (GSE), Eq. (16).

#### a. Calculation of $f_p$ coefficients

We have

$$f_p(\vec{T}, z) = \mathbb{E}_{\{\Phi_Q \sim \text{Haar}(\mathcal{H}_Q)\}} \left[ p(z) \prod_{Q_A} p(Q_A|z)^{T_{Q_A}} \right] = \mathbb{E}_{\{\Phi_Q \sim \text{Haar}(\mathcal{H}_Q)\}} \left[ \left( \sum_{Q_A} p(Q_A, z) \right)^{1-k} \prod_{Q_A} p(Q_A, z)^{T_{Q_A}} \right], \quad (\text{B12})$$

where we expressed everything in terms of the joint distribution  $p(Q_A, z)$ , Eq. (B3). To make progress, we adopt a replica limit approach: we set  $1 - k \mapsto n$ , compute the integral for positive integer  $n$ , then take the limit  $n \rightarrow 1 - k$  in the result.

By expanding the  $n$ -th power of the multinomial, we obtain

$$f_p^{(n)}(\vec{T}, z) = \sum_{\vec{T}' \in \mathcal{T}(n, N)} \binom{n}{\vec{T}'} \mathbb{E}_{\{\Phi_Q \sim \text{Haar}(\mathcal{H}_Q)\}} \prod_{Q_A} p(Q_A, z)^{T_{Q_A} + T'_{Q_A}}. \quad (\text{B13})$$

Now we note that

$$p(Q_A, z) = \langle \Psi | (\hat{\Pi}_{Q_A} \otimes |z\rangle\langle z|) | \Psi \rangle = p(Q_A + Q_B(z)) \langle \Phi_{Q_A + Q_B(z)} | (\hat{\Pi}_{Q_A} \otimes |z\rangle\langle z|) | \Phi_{Q_A + Q_B(z)} \rangle, \quad (\text{B14})$$

i.e., the probability  $p(Q_A, z)$  depends only on one charge component of  $|\Psi\rangle$ , namely  $Q = Q_A + Q_B(z)$ , with  $Q_B(z) = \sum_{i=1}^{N_B} z_i$  the total charge of bit string  $z$  on  $B$ . This allows us to factor the average as

$$f_p^{(n)}(\vec{T}, z) = \sum_{\vec{T}' \in \mathcal{T}(n, N)} \binom{n}{\vec{T}'} \prod_{Q_A} \mathbb{E}_{\Phi_{Q_A + Q_B(z)}} \left[ p(Q_A, z)^{T_{Q_A} + T'_{Q_A}} \right]. \quad (\text{B15})$$

The calculation thus reduces to the Haar average

$$\mathbb{E}_{\Phi_Q \sim \text{Haar}(\mathcal{H}_Q)} \langle \Phi_Q | (\mathbb{I}_A \otimes |z\rangle\langle z|_B) | \Phi_Q \rangle^\ell = \text{Tr} \left( (\mathbb{I}_A \otimes |z\rangle\langle z|_B)^{\otimes \ell} \rho_{\text{Haar}, AB, Q}^{(\ell)} \right) \quad (\text{B16})$$

with  $\rho_{\text{Haar}, AB, Q}^{(\ell)}$  the moment of the Haar ensemble on the charge sector  $Q$  for the whole system  $AB$ , for arbitrary integer  $\ell$  (to be set to  $T_Q + T'_Q$  later). Note the projector  $\hat{\Pi}_{Q_A}$  on  $A$  is redundant as both  $Q$  and  $Q_B$  are fixed. Writing out  $\rho_{\text{Haar}, AB, Q}^{(\ell)}$  in terms of permutations, we have

$$\mathbb{E}_{\Phi_Q \sim \text{Haar}(\mathcal{H}_Q)} \langle \Phi_Q | (\mathbb{I}_A \otimes |z\rangle\langle z|_B) | \Phi_Q \rangle^\ell = \frac{[(\binom{N}{Q}) - 1]!}{[(\binom{N}{Q}) - 1 + \ell]!} \sum_{\sigma \in S_k} \text{Tr} \left( (\mathbb{I}_A \otimes |z\rangle\langle z|_B)^{\otimes \ell} \hat{\sigma}_{AB, Q} \right). \quad (\text{B17})$$

with  $\hat{\sigma}_{AB, Q}$  the permutation operator acting on charge sector  $Q$  of the total system  $AB$ . We have  $\text{Tr} \left( (\mathbb{I}_A \otimes |z\rangle\langle z|_B)^{\otimes \ell} \hat{\sigma}_{AB, Q} \right) = \text{Tr}_A \langle z|_B^{\otimes \ell} \hat{\sigma}_{AB, Q} |z\rangle_B^{\otimes \ell} = \hat{\sigma}_{A, Q_A}$ , i.e. the replica permutation acting on charge sector  $Q_A = Q - Q_B(z)$  on subsystem  $A$  only. This allows us to resum the expression exactly, obtaining

$$\mathbb{E}_{\Phi_Q \sim \text{Haar}(\mathcal{H}_Q)} \langle \Phi_Q | (\mathbb{I}_A \otimes |z\rangle\langle z|_B) | \Phi_Q \rangle^\ell = \frac{[(\binom{N}{Q}) - 1]!}{[(\binom{N}{Q}) - 1 + \ell]!} \frac{[(\binom{N_A}{Q_A}) - 1 + \ell]!}{[(\binom{N_A}{Q_A}) - 1]!}, \quad (\text{B18})$$

with  $Q = Q_A + Q_B(z)$ . We conclude that

$$f_p^{(n)}(\vec{T}, z) = \sum_{\vec{T}' \in \mathcal{T}(n, N)} \binom{n}{\vec{T}'} \prod_{Q_A=0}^{N_A} \left[ p(Q)^{T_{Q_A} + T'_{Q_A}} \frac{[(\binom{N}{Q}) - 1]!}{[(\binom{N_A}{Q_A}) - 1]!} \frac{[(\binom{N_A}{Q_A}) - 1 + T_{Q_A} + T'_{Q_A}]!}{[(\binom{N}{Q}) - 1 + T_{Q_A} + T'_{Q_A}]!} \right]_{Q=Q_A+Q_B(z)}. \quad (\text{B19})$$

### b. Approximation and replica limit

Unfortunately, the replica limit  $n \rightarrow 1 - k$  in Eq. (B19) does not appear to be tractable. To make progress, we make a further approximation: we assume that  $\binom{N}{Q}, \binom{N_A}{Q_A} \gg 1$ , and approximate the ratios of factorials as

$$\frac{[(\binom{N}{Q}) - 1]!}{[(\binom{N}{Q}) - 1 + \ell]!} \frac{[(\binom{N_A}{Q_A}) - 1 + \ell]!}{[(\binom{N_A}{Q_A}) - 1]!} \approx \left[ \binom{N_A}{Q_A} \binom{N}{Q}^{-1} \right]^\ell. \quad (\text{B20})$$

This approximation neglects terms of order  $\ell^2 / \binom{N_A}{Q_A}, \ell^2 / \binom{N}{Q}$ . Since the replica limit  $n \rightarrow 1 - k$  in principle depends on all integer values of the replica number  $n$ , and  $\ell = T_{Q_A} + T'_{Q_A}$  can take on values up to the total number of replicas  $n + k$  (which is unbounded), this approximation is not rigorously justified. In effect, we are taking the  $N, N_A \rightarrow \infty$  limit before the replica limit  $n \rightarrow 1 - k$ , where in reality the opposite order should be followed. For this reason, the following analysis is non-rigorous and serves only to produce a conjecture for the form of the target ensemble, which has to then be checked numerically or through other means.

Within the approximation in Eq. (B20), we get

$$\begin{aligned} f_p^{(n)}(\vec{T}, z) &\simeq \sum_{\vec{T}' \in \mathcal{T}(n, N)} \binom{n}{\vec{T}'} \prod_{Q_A} \left[ p(Q) \binom{N_A}{Q_A} \binom{N}{Q}^{-1} \right]^{T_{Q_A} + T'_{Q_A}} \\ &= \left[ \sum_{Q_A} p(Q) \binom{N_A}{Q_A} \binom{N}{Q}^{-1} \right]^n \prod_{Q_A} \left[ p(Q) \binom{N_A}{Q_A} \binom{N}{Q}^{-1} \right]^{T_{Q_A}}, \end{aligned} \quad (\text{B21})$$

using  $Q$  as shorthand for  $Q_A + Q_B(z)$ . Now we can straightforwardly take the  $n \rightarrow 1 - k$  replica limit:

$$f_p(\vec{T}, z) \simeq \left( \sum_{Q_A} p(Q) \binom{N_A}{Q_A} \binom{N}{Q}^{-1} \right) \prod_{Q_A} \left[ \frac{p(Q) \binom{N_A}{Q_A} \binom{N}{Q}^{-1}}{\sum_{Q'_A} p(Q') \binom{N_A}{Q'_A} \binom{N}{Q'}^{-1}} \right]^{T_{Q_A}}, \quad (\text{B22})$$

Finally, recalling the the probability distribution  $\pi_p(Q, Q_B) = p(Q) \binom{N_A}{Q_A} \binom{N_B}{Q_B} \binom{N}{Q}^{-1}$  and its marginals, we can rewrite the expression as

$$\begin{aligned} f_p(\vec{T}, z) &\simeq \binom{N_B}{Q_B}^{-1} \left( \sum_{Q_A} \pi_p(Q, Q_B) \right) \prod_{Q_A} \left( \frac{\pi_p(Q_B, Q)}{\sum_{Q'_A} \pi_p(Q', Q_B)} \right)^{T_{Q_A}} \\ &= \binom{N_B}{Q_B}^{-1} \pi_p(Q_B) \prod_{Q_A} [\pi_p(Q_A + Q_B | Q_B)]^{T_{Q_A}}. \end{aligned} \quad (\text{B23})$$

c. *Reverse-engineering the ensemble from the moment operators*

Plugging the approximate result Eq. (B23) back into Eq. (B9) gives

$$\rho_{\text{target}}^{(k)} \simeq \sum_{Q_B} \pi_p(Q_B) \hat{\Pi}_{\text{sym}}^{(k)} \left( \sum_{\vec{T} \in \mathcal{T}(k, N)} \binom{k}{\vec{T}}^2 \bigotimes_{Q_A=0}^{N_A} \pi_p(Q_A + Q_B | Q_B)^{T_{Q_A}} \rho_{\text{Haar}, A, Q_A}^{(T_{Q_A})} \right) \hat{\Pi}_{\text{sym}}^{(k)} \quad (\text{B24})$$

(note that Eq. (B23) depends on  $z$  only through  $Q_B(z)$ , so the sum over  $z$  cancels out the  $\binom{N_B}{Q_B}^{-1}$  prefactor). From these moment operators, it is possible to “reverse-engineer” the form of the ensemble. Two key observations can guide us:

1. The moment operator is in the form  $\rho_{\text{target}}^{(k)} = \sum_{Q_B} \pi_p(Q_B) \rho_{\text{target}, Q_B}^{(k)}$ , which implies the target ensemble  $\mathcal{E}_{\text{target}}$  is a stochastic mixture of multiple ensembles  $\mathcal{E}_{\text{target}, Q_B}$ , each one weighted by a probability  $\pi_p(Q_B)$  (in other words: to sample a state from  $\mathcal{E}_{\text{target}}$ , first sample  $Q_B \sim \pi_p$ , then sample a state from  $\mathcal{E}_{\text{target}, Q_B}$ ).
2. For each value of  $Q_B$ , we note that the moment operator  $\rho_{\text{target}, Q_B}^{(k)}$  is a product of Haar moment operators in different charge sectors, with each sector  $Q_A$  weighted by a factor of  $\pi_p(Q_A + Q_B | Q_B)$ .

Building on these observations, it is possible to formulate a recipe to sample from a target ensemble  $\mathcal{E}_{\text{target}}$  whose moment operators are as in Eq. (B24):

- (i) Draw a value of  $Q_B \sim \pi_p(Q_B)$ ;
- (ii) Draw a collection of Haar-random states  $\{|\phi_{Q_A}\rangle\}_{Q_A}$  in each charge sector  $Q_A$  of the subsystem;
- (iii) Output the state

$$|\psi\rangle = \sum_{Q_A} \sqrt{\pi_p(Q_A + Q_B | Q_B)} |\phi_{Q_A}\rangle. \quad (\text{B25})$$

Finally, since our derivation is valid only in the limit of large Hilbert space dimensions  $\binom{N_A}{Q_A} \gg 1$ , the above recipe can be further simplified and reduced to the GSE, Eq. (16). We note that the output state in Eq. (B25) equals

$$|\psi\rangle = \sum_{Q_A} \sqrt{\pi_p(Q_A + Q_B | Q_B)} |\phi_{Q_A}\rangle = \frac{[\bar{\rho}_p(Q_B)]^{1/2} |\xi\rangle}{\langle \xi | \bar{\rho}_p(Q_B) | \xi \rangle^{1/2}}, \quad (\text{B26})$$

where

$$|\xi\rangle = 2^{-N_A/2} \bigoplus_{Q_A} \binom{N_A}{Q_A}^{1/2} |\phi_{Q_A}\rangle, \quad (\text{B27})$$

$$\bar{\rho}_p(Q_B) = \sum_{Q_A=0}^{N_A} \pi_p(Q_A + Q_B | Q_B) \frac{\hat{\Pi}_{Q_A}}{\text{Tr}(\hat{\Pi}_{Q_A})}. \quad (\text{B28})$$



In words,  $|\xi\rangle$  is a random state with *fixed* charge distribution  $p(Q_A) = 2^{-N_A} \binom{N_A}{Q_A}$ , and  $|\psi\rangle$  is a “ $\rho$ -distortion” of  $|\xi\rangle$  by the density matrix  $\bar{\rho}_p(Q_B)$ . But in the limit of large charge sectors  $\binom{N_A}{Q_A} \gg 1$ , the constraint on the charge distribution of  $|\xi\rangle$  becomes unimportant: expressing a Haar-random state on  $A$  as  $\sum_{Q_A} \sqrt{p(Q_A)} |\phi_{Q_A}\rangle$ , one would find  $p(Q_A) \approx 2^{-N_A} \binom{N_A}{Q_A}$  almost surely. Specifically, we have

$$\mathbb{E}_{\psi \sim \text{Haar}(\mathcal{H}_A)} \left[ \left( p(Q_A) - 2^{-N_A} \binom{N_A}{Q_A} \right)^2 \right] = 2^{-2N_A} \binom{N_A}{Q_A}^2 \left[ \frac{1 + \binom{N_A}{Q_A}^{-1}}{1 + 2^{-N_A}} - 1 \right], \quad (\text{B29})$$

corresponding to a relative error on  $p(Q_A)$  of order  $\binom{N_A}{Q_A}^{-1/2}$ , which we assumed small.

Thus the state  $|\xi\rangle$ , Eq. (B27), becomes indistinguishable from an unconstrained Haar-random state on the whole Hilbert space in the limit of large  $N_A$ . Since  $\rho$ -distortion of the Haar ensemble gives the Scrooge ensemble, what we just described is a stochastic mixture of Scrooge ensembles, i.e. a GSE (note also that the factor of  $2^{N_A} \langle \psi | \rho | \psi \rangle$ , which modifies the measure in the definition of the Scrooge ensemble, concentrates around 1 exponentially with increasing  $N_A$  and so can be neglected in this same limit). The GSE is specified by the distribution  $\pi_p(Q_B)$  and the density matrices  $\{\bar{\rho}_p(Q_B)\}$ , Eq. (B28).

#### 4. Charge-non-revealing measurements on symmetric states

Here we focus on the case of  $X$ -basis measurements ( $b \mapsto x$ ) on initial states with well-defined charge, i.e., we assume  $p(Q) = \delta_{Q, Q_0}$  for some fixed value  $Q_0$ . We will follow the same strategy as in the previous case, and will obtain as a result a standard (non-generalized) Scrooge ensemble determined uniquely by the value of  $Q_0$ . In the special case of  $Q_0 = N/2$  (charge neutrality), this will reduce to the Haar ensemble.

##### a. Calculation of $f_p$ coefficients

In this case, the general form of the projected ensemble’s moment operators, Eq. (B9) depends on coefficients

$$f_p(\vec{T}, x) = \mathbb{E}_{\Phi_{Q_0} \sim \text{Haar}(\mathcal{H}_{Q_0})} \left[ p(x) \prod_{Q_A} p(Q_A | x)^{T_{Q_A}} \right] = \mathbb{E}_{\Phi_{Q_0} \sim \text{Haar}(\mathcal{H}_{Q_0})} \left[ p(+) \prod_{Q_A} p(Q_A | +)^{T_{Q_A}} \right]. \quad (\text{B30})$$

Here, using the invariance of the measure under  $U(1)$ -symmetric unitaries, we have absorbed a unitary  $\bigotimes_i Z_i^{x_i}$  to map any measurement outcome  $|x\rangle$  to  $|+\rangle^{\otimes N_B}$ . In this derivation we will drop the tensor power from the notation and just write  $|+\rangle$  in lieu of  $|+\rangle^{\otimes N_B}$ . Following the same replica approach used for the case of  $Z$  measurements before, we can define

$$\begin{aligned} f_p^{(n)}(\vec{T}, +) &= \mathbb{E}_{\Phi_{Q_0} \sim \text{Haar}(\mathcal{H}_{Q_0})} \left[ \left( \sum_{Q_A} p(Q_A, +) \right)^n \prod_{Q_A} p(Q_A, +)^{T_{Q_A}} \right] \\ &= \sum_{\vec{T}' \in \mathcal{T}(n, N)} \binom{n}{\vec{T}'} \mathbb{E}_{\Phi_{Q_0} \sim \text{Haar}(\mathcal{H}_{Q_0})} \left[ \prod_{Q_A} p(Q_A, +)^{T_{Q_A} + T'_{Q_A}} \right] \end{aligned} \quad (\text{B31})$$

The argument of the Haar average can now be written as

$$\prod_{Q_A=0}^{N_A} p(Q_A, +)^{\ell(Q_A)} = \langle \Phi_{Q_0} |^{\otimes r} \left( \bigotimes_{Q_A=0}^{N_A} \hat{\Pi}_{Q_A}^{\otimes \ell(Q_A)} \otimes |+\rangle \langle +|^{\otimes r} \right) | \Phi_{Q_0} \rangle^{\otimes r}, \quad (\text{B32})$$

with  $r = n + k$  the total number of replicas and  $\ell(Q_A) = T_{Q_A} + T'_{Q_A}$ . Thus the average yields

$$\mathbb{E}_{\Phi_{Q_0} \sim \text{Haar}(\mathcal{H}_{Q_0})} \left[ \prod_{Q_A} p(Q_A, +)^{\ell(Q_A)} \right] = \frac{[(\binom{N}{Q_0}) - 1]!}{[(\binom{N}{Q_0}) - 1 + r]!} \sum_{\sigma \in S_r} \text{Tr} \left[ \hat{\sigma}_{AB, Q_0} \left( \bigotimes_{Q_A=0}^{N_A} \hat{\Pi}_{Q_A}^{\otimes \ell(Q_A)} \otimes |+\rangle \langle +|^{\otimes r} \right) \right], \quad (\text{B33})$$

with  $\hat{\sigma}_{AB, Q_0}$  the replica permutation operator acting on charge sector  $Q_0$  of the whole system  $AB$ . This equals  $\hat{\sigma}_{AB} \hat{\Pi}_{Q_0}^{\otimes r}$ , with  $\hat{\sigma}_{AB}$  the replica permutation acting on the whole Hilbert space of  $AB$  (not just sector  $Q_0$ ); in turn, this factors across the Hilbert spaces of the two subsystems, so in all  $\hat{\sigma}_{AB, Q_0} = (\hat{\sigma}_A \otimes \hat{\sigma}_B) \hat{\Pi}_{Q_0}^{\otimes r}$ . Thus we have

$$\begin{aligned} \text{Tr} \left[ \hat{\sigma}_{AB, Q_0} \left( \bigotimes_{Q_A=0}^{N_A} \hat{\Pi}_{Q_A}^{\otimes \ell(Q_A)} \otimes |+\rangle\langle +|^{\otimes r} \right) \right] &= \text{Tr} \left[ (\hat{\sigma}_A \otimes \hat{\sigma}_B) \left( \bigotimes_{Q_A=0}^{N_A} (\hat{\Pi}_{Q_A} \otimes \hat{\Pi}_{Q_B})^{\otimes \ell(Q_A)} \right) (\mathbb{I}_A \otimes |+\rangle\langle +|^{\otimes r}) \right] \\ &= \text{Tr}_A \left[ \hat{\sigma}_A \bigotimes_{Q_A} \hat{\Pi}_{Q_A}^{\otimes \ell(Q_A)} \right] \langle +|^{\otimes r} \hat{\sigma}_B \bigotimes_{Q_A} \hat{\Pi}_{Q_0-Q_A}^{\otimes \ell(Q_A)} |+\rangle^{\otimes r} \\ &= \text{Tr}_A \left[ \hat{\sigma}_A \bigotimes_{Q_A} \hat{\Pi}_{Q_A}^{\otimes \ell(Q_A)} \right] \prod_{Q_A} \langle + | \hat{\Pi}_{Q_0-Q_A} | + \rangle^{\ell(Q_A)} \end{aligned} \quad (\text{B34})$$

where we used the fact that  $\hat{\Pi}_{Q_0} (\hat{\Pi}_{Q_A} \otimes \mathbb{I}_B) = \hat{\Pi}_{Q_A} \otimes \hat{\Pi}_{Q_B}$  with  $Q_B = Q_0 - Q_A$ , and that  $|+\rangle^{\otimes r}$  is invariant under replica permutations.

Now we will analyze the two terms in Eq. (B34). Starting with the second term, we have

$$\langle + | \hat{\Pi}_{Q_B} | + \rangle = \sum_{z: Q_B(z)=Q_B} |\langle + | z \rangle|^2 = 2^{-N_B} \binom{N_B}{Q_B}, \quad (\text{B35})$$

which is independent of the permutation  $\sigma$ . For the first term, we note that it vanishes if  $\sigma$  connects two replicas with a different value of  $Q_A$ , since in that case one gets a product of orthogonal projectors  $\hat{\Pi}_{Q_A} \hat{\Pi}_{Q'_A} = 0$  if  $Q_A \neq Q'_A$ . This restricts  $\sigma$  to be a product of permutations that only mix replicas with the same value of  $Q_A$ :  $\sigma \in S_{\ell(0)} \times S_{\ell(1)} \times \dots \times S_{\ell(N_A)}$  (for cases where  $\ell(Q_A) = 0$  we take  $S_0$  to be the trivial group). With this restriction on  $\sigma$ , we obtain

$$\begin{aligned} \sum_{\sigma \in S_r} \text{Tr}_A \left[ \hat{\sigma}_A \bigotimes_{Q_A} \hat{\Pi}_{Q_A}^{\otimes \ell(Q_A)} \right] &= \prod_{Q_A} \sum_{\sigma \in S_{\ell(Q_A)}} \text{Tr}_A \left[ \hat{\sigma}_A \hat{\Pi}_{Q_A}^{\otimes \ell(Q_A)} \right] \\ &= \prod_{Q_A} \sum_{\sigma \in S_{\ell(Q_A)}} \text{Tr}_A(\hat{\sigma}_{A, Q_A}) \\ &= \prod_{Q_A} \frac{[(\binom{N_A}{Q_A}) - 1 + \ell(Q_A)]!}{[(\binom{N_A}{Q_A}) - 1]!} \text{Tr}(\rho_{\text{Haar}, A, Q_A}^{\ell(Q_A)}) \\ &= \prod_{Q_A} \frac{[(\binom{N_A}{Q_A}) - 1 + \ell(Q_A)]!}{[(\binom{N_A}{Q_A}) - 1]!}, \end{aligned} \quad (\text{B36})$$

where we carried out the sum over permutations by composing the  $\ell(Q_A)$ -th moment operator for the Haar ensemble in each charge sector.

Plugging these results back in the expression for  $f_p^{(n)}(\vec{T}, +)$  yields

$$f_p^{(n)}(\vec{T}, +) = \frac{[(\binom{N}{Q_0}) - 1]!}{[(\binom{N}{Q_0}) - 1 + r]!} 2^{-rN_B} \sum_{\vec{T}' \in \mathcal{T}(n, N)} \binom{n}{\vec{T}'} \prod_{Q_A=0}^{N_A} \binom{N_B}{Q_0 - Q_A}^{T_{Q_A} + T'_{Q_A}} \frac{[(\binom{N_A}{Q_A}) - 1 + T_{Q_A} + T'_{Q_A}]!}{[(\binom{N_A}{Q_A}) - 1]!}. \quad (\text{B37})$$

### b. Approximation and replica limit

Again, Eq. (B37) is not directly amenable to a replica limit  $n \rightarrow 1 - k$ . However, if we take the limit of large Hilbert space dimension  $\binom{N_A}{Q_A} \rightarrow \infty$  before the replica limit, we can approximate

$$\frac{[(\binom{N_A}{Q_A}) - 1 + T_{Q_A} + T'_{Q_A}]!}{[(\binom{N_A}{Q_A}) - 1]!} \simeq \binom{N_A}{Q_A}^{T_{Q_A} + T'_{Q_A}}. \quad (\text{B38})$$

This allows an exact (within the large- $N_A$  limit) resummation of Eq. (B37),

$$\begin{aligned} f_p^{(n)}(\vec{T}, +) &\simeq \frac{[(\binom{N}{Q_0}) - 1]!}{[(\binom{N}{Q_0}) - 1 + r]!} 2^{-rN_B} \sum_{\vec{T}' \in \mathcal{T}(n, N)} \binom{n}{\vec{T}'} \prod_{Q_A=0}^{N_A} \left[ \binom{N_B}{Q_0 - Q_A} \binom{N_A}{Q_A} \right]^{T_{Q_A} + T'_{Q_A}} \\ &= \frac{[(\binom{N}{Q_0}) - 1]!}{[(\binom{N}{Q_0}) - 1 + r]!} 2^{-rN_B} \left( \sum_{Q_A} \binom{N_B}{Q_0 - Q_A} \binom{N_A}{Q_A} \right)^n \prod_{Q_A=0}^{N_A} \left[ \binom{N_B}{Q_0 - Q_A} \binom{N_A}{Q_A} \right]^{T_{Q_A}}. \end{aligned} \quad (\text{B39})$$

We can now take  $n \rightarrow 1 - k$  (and  $r = n + k \rightarrow 1$ ) and, using the identity  $\sum_{Q_A} \binom{N_A}{Q_A} \binom{N - N_A}{Q_0 - N_A} = \binom{N}{Q_0}$ , we obtain

$$f_p(\vec{T}, +) \simeq 2^{-N_B} \prod_{Q_A=0}^{N_A} \left[ \binom{N_B}{Q_0 - Q_A} \binom{N_A}{Q_A} \binom{N}{Q_0}^{-1} \right]^{T_{Q_A}} = 2^{-N_B} \prod_{Q_A=0}^{N_A} \pi(Q_A | Q_0)^{T_{Q_A}}, \quad (\text{B40})$$

with  $\pi(Q_A | Q_0) = \binom{N_A}{Q_A} \binom{N_B}{Q_0 - Q_A} \binom{N}{Q_0}^{-1}$ .

### c. Reverse-engineering the ensemble from the moment operators

Plugging the approximate result Eq. (B40) back into the general expression for moment operators Eq. (B9) gives

$$\rho_{\text{target}}^{(k)} \simeq \hat{\Pi}_{\text{sym}}^{(k)} \left( \sum_{\vec{T} \in \mathcal{T}(k, N)} \binom{k}{\vec{T}}^2 \bigotimes_{Q_A=0}^{N_A} \pi(Q_A | Q_0)^{T_{Q_A}} \rho_{\text{Haar}, A, Q_A}^{(T_{Q_A})} \right) \hat{\Pi}_{\text{sym}}^{(k)} \quad (\text{B41})$$

(the summation over  $x$  cancels the  $2^{-N_B}$  prefactor). Following the same steps as in the case of  $z$ -basis measurements, we can show that this moment operator corresponds to an ensemble obtained by drawing a collection of Haar-random states  $\{|\phi_{Q_A}\rangle\}$  in each charge sector and then outputting

$$|\psi\rangle = \sum_{Q_A} \sqrt{\pi(Q_A | Q_0)} |\phi_{Q_A}\rangle = \frac{[\bar{\rho}(Q_0)]^{1/2} |\xi\rangle}{\langle \xi | \bar{\rho}(Q_0) | \xi \rangle^{1/2}}, \quad (\text{B42})$$

where

$$|\xi\rangle = 2^{-N_A/2} \bigoplus_{Q_A} \binom{N_A}{Q_A}^{1/2} |\phi_{Q_A}\rangle, \quad (\text{B43})$$

$$\bar{\rho}(Q_0) = \sum_{Q_A=0}^{N_A} \pi(Q_A | Q_0) \frac{\hat{\Pi}_{Q_A}}{\text{Tr}(\hat{\Pi}_{Q_A})} = \sum_{Q_A} \binom{N_B}{Q_0 - Q_A} \binom{N}{Q_0}^{-1} \hat{\Pi}_{Q_A}. \quad (\text{B44})$$

In the limit  $N_A \rightarrow \infty$ , the states  $|\xi\rangle$  become Haar-distributed, so this is a  $\rho$ -distortion of the Haar ensemble, i.e., a Scrooge ensemble. The Scrooge ensemble is fully specified by the density matrix  $\bar{\rho}(Q_0)$ , which in turn depends only on the charge of the input state. In the special case of  $Q_0 = N/2$  (charge neutrality) and in the limit  $N \rightarrow \infty$ , the density matrix  $\bar{\rho}(N/2)$  becomes close to the identity, and we recover the Haar ensemble. Values of  $Q_0$  above or below neutrality will yield a Scrooge ensemble with a bias toward higher or lower charge, respectively.

### d. Typical initial states

Thus far we have computed the average of the moment operators over generator states  $\Phi_{Q_0}$  belonging to a given charge sector  $Q_0$ ,

$$\rho_{\text{target}}^{(k)} = \mathbb{E}_{\Phi_{Q_0} \sim \text{Haar}(\mathcal{H}_{Q_0})} \left[ \rho_{\mathcal{E}(\Phi_{Q_0})}^{(k)} \right], \quad (\text{B45})$$

and conjectured that the projected ensemble constructed from a *typical* state  $\Phi_{Q_0}$  should have moments close to  $\rho_{\text{target}}^{(k)}$ . However, as long as the state has a nontrivial charge density (that is,  $Q_0 = \sigma_0 N$  with  $0 < \sigma_0 < 1$ ), we can

prove this conjecture by using the method based on Levy's lemma (Lemma 1 in Appendix A), already applied in our proof of Theorem 1 following Ref. [8].

The proof in Ref. [8] carries over straightforwardly to our case by replacing the total Hilbert space dimension  $d$  by the dimension of the relevant charge sector,  $d_{Q_0} = \binom{N}{Q_0} = 2^{NH_2(\sigma_0) + o(N)}$ , with  $H_2(\sigma_0) = -\sigma_0 \log_2(\sigma_0) - (1-\sigma_0) \log_2(1-\sigma_0)$  the binary entropy. This dimension is still exponential in  $N$  provided  $\sigma_0 \neq 0, 1$ , guaranteeing the desired concentration of measure as  $N \rightarrow \infty$  (with  $\sigma_0$  fixed). For the Lipschitz constant  $\eta$  we may use the same value  $\eta = 2(2k-1)$  derived in Ref. [8]. Indeed we have

$$\sup_{x \neq y \in \mathcal{H}_{Q_0}} \frac{|f(x) - f(y)|}{\|x - y\|_2} \leq \sup_{x \neq y \in \mathcal{H}} \frac{|f(x) - f(y)|}{\|x - y\|_2} \leq \eta, \quad (\text{B46})$$

where with a slight abuse of notation we wrote  $x \in \mathcal{H}$  to denote  $x \in \mathbb{S}^{2\dim(\mathcal{H})-1}$  (the real unit vector corresponding to a complex normalized wavefunction in the Hilbert space). The first inequality follows trivially from  $\mathcal{H}_{Q_0} \subset \mathcal{H}$  while the second from the definition of Lipschitz constant. In words, a charge sector subspace defines a hypersphere  $\mathbb{S}^{2d_{Q_0}-1}$ , which is a submanifold of the hypersphere  $\mathbb{S}^{2d-1}$  associated to the whole Hilbert space; thus the moment operator restricted to symmetric generator states is still an (entry-wise) Lipschitz-continuous function with a Lipschitz constant no larger than  $\eta$ . The proof then proceeds unchanged except for the replacement  $d \mapsto d_{Q_0}$ .

This proves that Haar-random states  $|\Phi_{Q_0}\rangle$  give rise to projected ensembles whose moment operators are very close to the average  $\rho_{\text{target}}^{(k)}$  with high probability. However, note that our derivation of the average  $\rho_{\text{target}}^{(k)}$  itself is non-rigorous (relying on a replica limit).

### Appendix C: Constraints from locality of the dynamics

Refs. [51, 60] have showed that not all  $U(1)$ -symmetric unitaries on an  $N$ -qubit Hilbert space can be generated from  $U(1)$ -symmetric interactions among  $k$  qubits, if  $k < N$ . This applies to the random circuit models we consider in Sec. V, where  $k = 2$  (note that geometric locality is unimportant since  $U(1)$ -symmetric 2-qubit gates include the SWAP gate). This calls into question the legitimacy of averaging the collection of states  $\{|\Phi_Q\rangle\}_{Q=0}^N$  independently over the Haar ensemble in each charge sector  $Q$ , as we do in Appendix B to derive the form of the target ensemble. Here we justify this procedure.

Let us denote the group generated by 2-local,  $U(1)$ -symmetric gates on  $N$  qubits by  $G_{U(1)}^{N,2}$ . This is a compact Lie group, so it admits a Haar measure. Our goal is to show that the Haar average over  $G_{U(1)}^{N,2}$  is equivalent, for our purposes, to the Haar average over the entire  $U(1)$ -symmetric subgroup of  $U(2^N)$ ,  $G_{U(1)}^{N,N}$ . Ref. [51] shows that  $G_{U(1)}^{N,2}$  contains  $\bigoplus_Q SU(\mathcal{H}_Q)$ —the group of block-diagonal unitaries that act on each charge sector  $\mathcal{H}_Q$  as elements of the special unitary group (i.e., with determinant equal to 1). However, the relative phases between different sectors are subject to nontrivial constraints, so that it is not possible to generate all of  $G_{U(1)}^{N,N} = \bigoplus_Q U(\mathcal{H}_Q)$ . For our purposes, these relative phases will be unimportant, as we show next.

**Lemma 2** *For any function  $f$  and any state  $|\Psi\rangle$ , we have*

$$\mathbb{E}_{U \sim \text{Haar}(G_{U(1)}^{N,2})} [f(U|\Psi\rangle\langle\Psi|U^\dagger)] = \mathbb{E}_{U \sim \text{Haar}(G_{U(1)}^{N,N})} [f(U|\Psi\rangle\langle\Psi|U^\dagger)], \quad (\text{C1})$$

*that is, as long as the unitary  $U$  acts on a pure state, locally-generated  $U(1)$ -symmetric unitaries are equivalent to general  $U(1)$ -symmetric unitaries.*

*Proof.* Using the fact that  $G_{U(1)}^{N,2}$  contains as a subgroup  $\bigoplus_Q SU(\mathcal{H}_Q)$ , and using the invariance of the Haar measure under right multiplication by elements of  $G_{U(1)}^{N,2}$ , we can change variable to  $U \mapsto UV$ , with  $V = \bigoplus V_Q$ , and  $V_Q \in SU(\mathcal{H}_Q)$ . Let us consider  $V_Q = \tilde{V}_Q [e^{i\theta_Q} |\Phi_Q\rangle\langle\Phi_Q| \oplus W_{\theta_Q}^\perp]$ , where  $\theta_Q$  is an arbitrary phase,  $W_{\theta_Q}^\perp$  is a unitary matrix on the orthogonal complement of  $|\Phi_Q\rangle$  in  $\mathcal{H}_Q$  of determinant  $e^{-i\theta_Q}$ , and  $\tilde{V}_Q$  is another unitary matrix in  $SU(\mathcal{H}_Q)$ . The action of  $V$  on the state  $|\Psi\rangle = \sum_Q \sqrt{p(Q)} |\Phi_Q\rangle$  is

$$V|\Psi\rangle = \sum_Q \sqrt{p(Q)} V_Q |\Phi_Q\rangle = \sum_Q \sqrt{p(Q)} e^{i\theta_Q} \tilde{V}_Q |\Phi_Q\rangle \quad (\text{C2})$$

which in turn is equivalent to that of a general matrix  $\bigoplus_Q e^{i\theta_Q} \tilde{V}_Q \in \bigoplus_Q U(\mathcal{H}_Q) = G_{U(1)}^{N,N}$ . ■

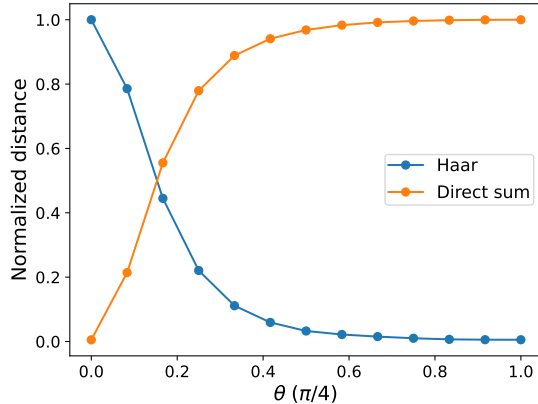


Figure 9. Late-time average of the second-moment distances between the projected ensemble and the Haar ensemble (blue) and the direct sum of Haar ensembles in the charge sectors (orange) as a function of  $\theta$  (parameter of the initial state) for  $N = 20$ ,  $N_A = 2$ .

#### Appendix D: Choice of parameters for numerical simulations

Here we discuss parameter choices for the numerical simulations of intermediate initial states, where we test the convergence to the GSE. First we justify the choice of  $\theta = \pi/20$  as a reasonable intermediate value between the Néel and  $X$ -basis state. In Fig. 9 we show the late-time average value of the distance  $\Delta^{(2)} = \|\rho_{\mathcal{E}}^{(2)} - \rho_{\text{target}}^{(2)}\|_{\text{tr}}$  between the projected ensemble and a target ensemble chosen to be either the Haar ensemble on the whole Hilbert space, or the weighted sum of Haar ensembles on the charge sectors, as in Eq. (32). As expected, the two target ensembles yield  $\Delta^{(2)} \simeq 0$  respectively at  $\theta = 0$  and  $\theta = \pi/4$ , but at intermediate  $\theta$  they both give a large value of  $\Delta^{(2)}$ . We choose  $\theta = \pi/20$  as it appears to be roughly equidistant from the two extremal ensembles.

Finally we provide some details on the numerical construction of the GSE moment operators. These are constructed numerically by sampling states  $|\psi\rangle \sim \mathcal{E}_{GSE}$  (according to the prescription in the main text)  $M$  times, and computing the approximate moment operator

$$\rho_{\text{app.},M}^{(k)} = \frac{1}{M} \sum_{m=1}^M |\psi_m\rangle\langle\psi_m|^{\otimes k}. \quad (\text{D1})$$

It is important to ensure that the number of samples  $M$  is adequate to guarantee convergence to the true GSE moment operator.

Since the Hilbert space of the subsystem A has dimension  $2^{N_A}$ , it is reasonable to expect that the number of sampled states needed to ensure convergence should grow rapidly with  $N_A$ . To investigate this question quantitatively, we focused on the  $|+\rangle^{\otimes N}$  initial state, where the form of the GSE reduces to the analytically tractable Haar ensemble, so as to have an exact benchmark to compare against. We calculated the distance between the sampled moment operator  $\frac{1}{M} \sum_{m=1}^M |\psi_m\rangle\langle\psi_m|^{\otimes 2}$  and the analytically constructed one,  $\rho_H^{(2)} = \binom{2^{N_A}-1}{2}^{-1} \hat{\Pi}_{\text{sym}}^{(2)}$ . Results shown in Fig. 10 show that the statistical error due to finite sampling  $M$  scales approximately as  $\sim 2^{N_A}/\sqrt{M}$ . This implies that reaching a target precision  $\epsilon$  requires  $M \sim 4^{N_A}/\epsilon^2$  samples. This is reasonable since a quantum state  $k$ -design on a Hilbert space of dimension  $d_A$  requires  $\Omega(d_A^k)$  [39], so  $4^{N_A} = d_A^2$  is the expected scaling for the case under consideration,  $k = 2$ . Since in Fig. 6 in the main text we consider  $N_A \leq 4$ , to ensure a negligible error  $\epsilon \lesssim 10^{-3}$  we set  $M = 2 \times 10^8$ .

#### Appendix E: Numerical results for higher moments

Here we report numerical evidence for deep thermalization at the level of higher moments  $k > 2$ . Fig. 11 shows data for moments  $k = 3$  and  $4$  for the setup considered in Sec. V A 3 and Fig. 6: maximally charge-revealing measurements on a state that is initialized to Eq. (30) with  $\theta = \pi/20$ , i.e., a product state in a local basis intermediate between  $x$  and  $z$ . The target ensemble is again set to the GSE. The third and fourth moment operators are computed by following the Monte Carlo method of Appendix D with  $M = 5 \times 10^7$  and  $2 \times 10^8$  samples respectively. Results are consistent with deep thermalization at all moments  $k$ .



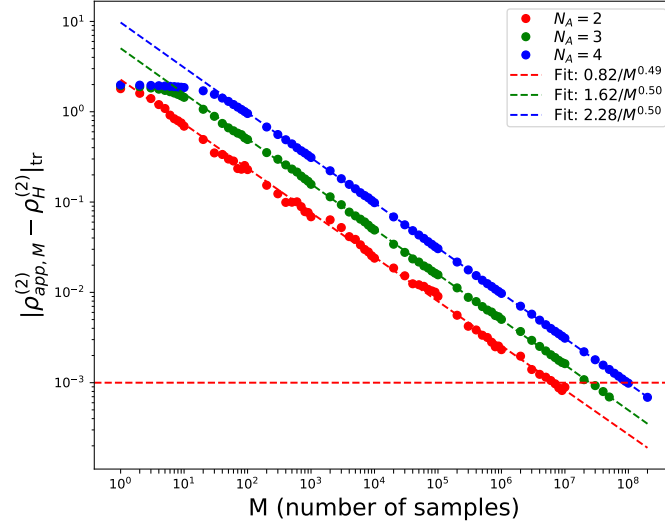


Figure 10. The distance  $\|\rho_{\text{app},M}^{(2)} - \rho_H^{(2)}\|$  between the sampled moment operator, Eq. (D1), and the true Haar moment operator is plotted against the number of samples  $M$ , for subsystem sizes  $N_A = 2, 3, 4$ . We see the expected decay in the number of samples as  $\sim M^{-1/2}$ , with a prefactor roughly proportional to  $2^{N_A}$ . A precision of  $\lesssim 10^{-3}$ , which is below the finite-size floor of  $\Delta^{(k)}$  for all cases studied in Fig. 6, is achieved for  $M \gtrsim 10^8$ .

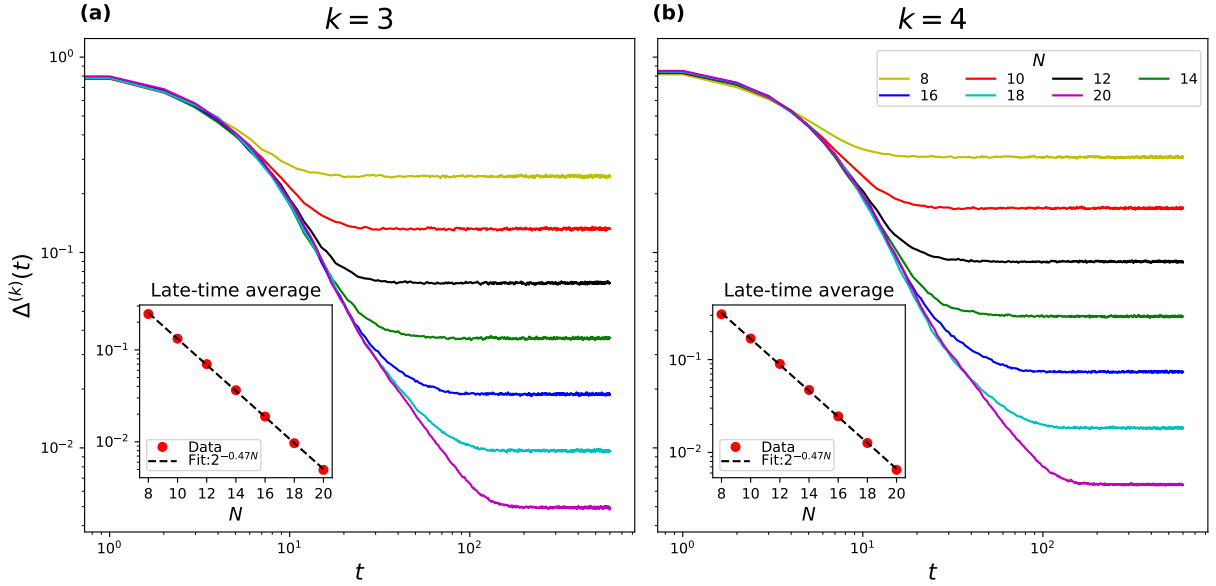


Figure 11. Trace distances  $\Delta^{(3)}$  (a) and  $\Delta^{(4)}$  (b) between the projected ensemble and the GSE constructed from the initial state of Eq. (30) with  $\theta = \pi/2$  and  $z$ -basis measurements, for  $N_A = 2$ . The setting is the same as in Fig. 6. The late-time saturation value of  $\Delta^{(3)}$  and  $\Delta^{(4)}$  decays exponentially in  $N$ , consistent with  $2^{-N/2}$  (inset).